UNIVERSITÀ DEGLI STUDI DI PADOVA
Facoltà di Scienze MM.NN.FF.
Facoltà di Ingegneria

ISTITUTO NAZIONALE DI FISICA NUCLEARE
Laboratori Nazionali di Legnaro

in collaboration with Confindustria Veneto

MASTER THESIS
in

"Surface Treatments for Industrial Applications"

WILL HIGH POWER IMPULSE MAGNETRON SPUTTERING (HIPIMS) BE THE RIGHT TECHNIQUE FOR Nb/Cu COATED 1.5GHz SUPERCONDUCTING CAVITIES?

Supervisor: Prof. V. Palmieri

Co-Supervisor: Dr. C. Pira

Student: Eng. Yin Meng
Matr. N. 938769

Academic Year 2009-10

Index

Abstract

Particle physics is now at the threshold of great discoveries. The experiments with particle accelerators and observations of the cosmos have focused attention on phenomena that can not be explained by the standard theory. The technology based on superconducting niobium accelerating cavities can reach a high expenditure of energy by many orders of magnitude lower than that of normal-conducting copper cavities. Even taking into account the power spent to maintain the temperature of liquid helium, the net gain in economic terms is still unassailable.

The sputtering technology was chosen first in the pure diode configuration and subsequently in the magnetron configuration. High Power Impulse Magnetron Sputtering (HIPIMS) is an evolution of the magnetron technique which relies on 100 μs high voltage pulses of the order of 1 kV compared to the 300 V of the standard DC magnetron process. During the pulse a huge power density is deposited onto the target, of the order of a few kW/cm^2 compared to a few W/cm^2 of the standard DC process, producing a highly dense plasma in which also the Nb atoms are partially ionized. These can in turn be attracted to the substrate with a suitable bias. A further advantage of the technique lies in the fact that no hardware changes are required compared to a standard DC biased magnetron system, except for the obvious replacement of the power supply.

In this work, an R&D effort has been undertaken to study the HIPIMS, to improve it and understand the correlation between the parameters applied and the film morphology, the superconducting properties and the RF film quality.

The experiment system is based on the NEW HIGH-RATE SYSTEM for the deposition cavity 1.5 GHz. The experimental details and the measurements of the characteristics of the deposited films are described. Even though the work is still in progress, all of the partial results from now on have been analyzed and commented, in order to extrapolate all the information. The final results are a global overview of the HIPIMS techniques for Nb on 1.5Hz superconducting cavity. Suggestions for future efforts have been included as part of the conclusions.

1 Introduction

1.1 Accelerating structures

A particle accelerator is a device that uses electromagnetic fields to propel charged particles to high speeds and to contain them in well-defined beams. [1] A linear particle accelerator (often shortened to linac) is a type of particle accelerator that greatly increases the velocity of charged subatomic particles or ions by subjecting the charged particles to a series of oscillating electric potentials along a linear beamline. [2]

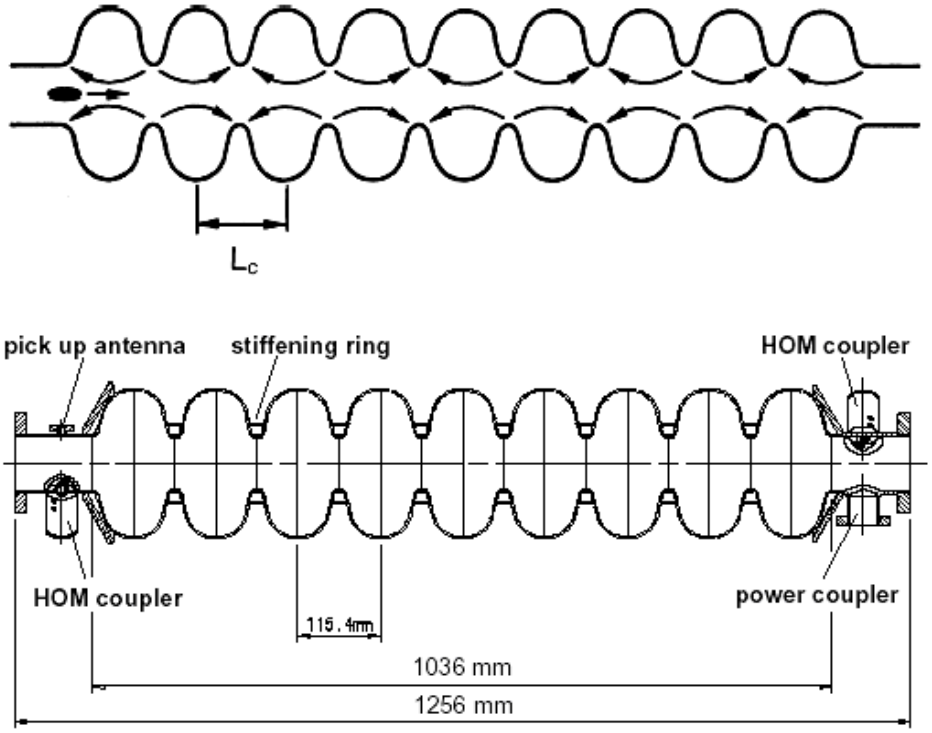

Figure 1.1 9-cells TESLA superconducting accelerator

Accelerating cavities are used to increase the energy of a charged particle beam. The energy gain per unit length is an important parameter of such devices.

The accelerating voltage:

$$V_{acc} = \left| \frac{1}{e} \times \text{energy gain during transit} \right| \tag{1.1}$$

For particles travelling with the velocity of light c on the symmetry axis in z–direction and an accelerating mode with eigenfrequency ω this gives:

$$V_{acc} = \left| \int_0^d E_z(z) e^{\frac{i\omega z}{c}} dz \right| \tag{1.2}$$

The key parameters of the superconducting accelerating structures are E_{acc}, E_{pk} and H_{pk}.

$$E_{acc} = \frac{V_{acc}}{d} \tag{1.3}$$

E_{pk} is the highest electric field inside the accelerating structure

H_{pk} is the highest magnetic field inside the accelerating structure

For a typical TESLA-type cavity, the theoretical maximum accelerating gradient is about 55 MV/m [3]. At the moment the standard E_{acc}, achievable in the industrial production, is about 25-30 MV/m for working TESLA-type accelerating cavities based on bulk niobium material.

In order to sustain the radiofrequency fields in the cavity, an alternating current is flowing in the cavity walls. This current dissipates power in the wall as it experiences a surface resistance.

The power which is dissipated in the cavity:

$$P_{diss} = \frac{1}{2} \oint_A R_s H_s^2 dA = \frac{1}{2} R_s \oint_A H_s^2 dA \tag{1.4}$$

where:

R_s is the global surface resistance

H_s is the magnetic field amplitude

The quality factor Q_0:

$$Q_0 = \frac{\omega U}{P_{diss}} \tag{1.5}$$

where:

U is the energy stored in the electromagnetic field in the

accelerating cavity:

$$U = \frac{1}{2}\mu_0 \oint_V H^2 dV \tag{1.6}$$

Also,

$$Q_0 = \frac{G}{R_s} \tag{1.7}$$

where:

G is the geometrical constant; it depends on the geometry of a cavity and field distribution of the excited mode

$$G = \frac{\omega\mu_0 \oint_V H^2 dV}{\oint_A H^2 dA} \tag{1.8}$$

The quality factor can also be defined as:

$$Q_0 = \frac{f}{\Delta f} \tag{1.9}$$

where:

f is the resonance frequency

Δf the full width at half height of the resonance curve in an unloaded cavity

One can see that the efficiency with which a particle beam can be accelerated in a radiofrequency cavity depends on the surface resistance. The smaller the resistance the lower the power dissipated in the cavity walls, the higher the radiofrequency power available for the particle beam. This is the fundamental advantage of superconducting cavities as their surface resistance is much lower and outweighs the power needed to cool the cavities to liquid helium temperatures.

1.2 Superconducting

Superconductivity is an electrical resistance of exactly zero which occurs in certain materials below a characteristic temperature. It is also characterized by a phenomenon called the Meissner effect, the ejection of any sufficiently weak magnetic field from the interior of the superconductor as it transitions into the superconducting state. The occurrence of the Meissner effect indicates that superconductivity cannot be understood simply as the idealization of perfect conductivity in classical physics. By now a large number of elements and compounds (mainly alloys and ceramics) have been found showing these behaviors.

Two different types of superconductors were discovered, called respectively type I and type II. They have certain common features, but differ also in some important ways. In addition, any external magnetic field up to a critical field $B < B_{crit}$ is expelled. This magnetic field expulsion is called the Meissner-Ochsenfeld effect. This behavior significantly differs from the properties of an ideal conductor where the field would be trapped inside the material. Even if the field is switched off, an ideal conductor would keep the magnetic field and become a permanent magnet as the currents induced by the field will continue to flow.

Experimentally, B_c can be determined from the area below the magnetization curve of the material. If the field exceeds a critical value B_c in superconductors of type I the superconductivity breaks down and the normal conducting state is restored.

This critical field depends on the critical temperature:

$$B_c(T) = B_c(0)\left[1-\left(\frac{T}{T_c}\right)^2\right] \tag{1.10}$$

For the second type of superconductor the magnetic field will start to penetrate the material above the lower critical field B_{c1}. Magnetic fluxons enter the material and their number increases with increasing field. If one raises the field further to a value of B_{c2} the material becomes normalconducting. The temperature dependence of the critical magnetic fields B_{c1} and B_{c2} is the same as for the B_c of a type I

superconductor.

For superconducting cavities niobium shows the most interesting properties. The general features of superconductivity as well as the special properties of niobium are described.

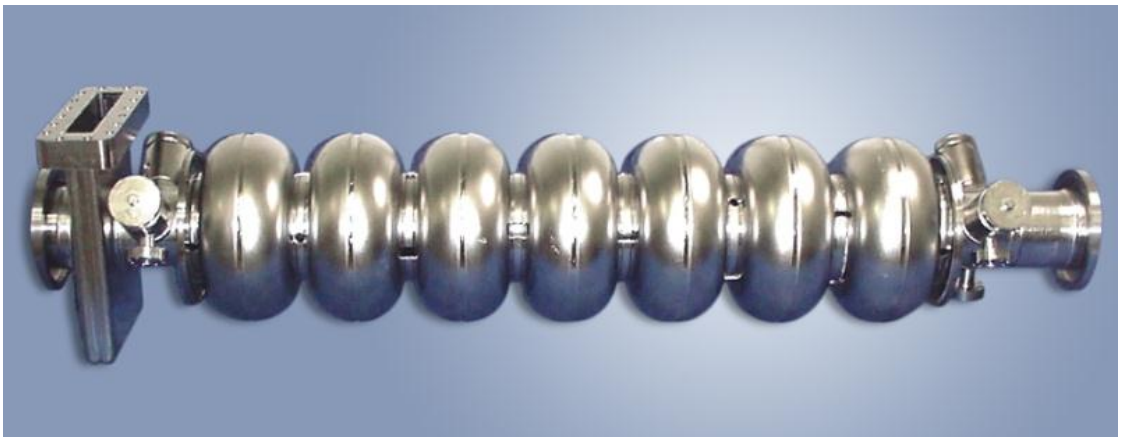

Figure 1.2 Superconducting accelerator structures of niobium

Niobium is a transition metal of V group and fifth period. It is a chemical element that has the symbol Nb and atomic number 41, Atomic weight 92.9 g/mol, Atomic radius 2.08. Its Density is 8570 kg m^3. A soft, gray, ductile transition metal, niobium is found in pyrochlore and columbite. It was first discovered in the latter mineral and so was initially named columbium; now that mineral is also called niobite. Niobium is also used in special steel alloys as well as in welding, nuclear industries, electronics, optics and jewelry. Niobium is pure element Type-II superconductors. In the family of superconducting element it has the highest critical temperature. Its crystalline lattice is B.C.C. and a is 3.3033Å. The critical temperature is 9.26K.

The Residual Resistivity Ratio also called RRR or triple-R and noted as β is the factor by which resistivity drops to the residual value. It is defined as: the ratio of the resistance of the magnet coil at 293K and the resistance of the magnet coil just above the transition temperature from superconducting to normal state. The Residual Resistivity Ratio is a measurement of the purity of a sample of metal [4]. It generally used for very precise measurements like experimentation. For Nb, it is defined as the ratio of the electrical resistivity at two temperatures: 273 K and 4.2 K. The value of

RRR indicates the purity and the low-temperature thermal conductivity of a material, and is often used as a material specification for superconductors.

For pure Nb used in radio-frequency cavities of linear accelerators, the low temperature resistivity is defined as the normal-state value extrapolated to 4.2 K, but this value doesn't differ much from the 10K value.

$$RRR = \frac{\rho(273K)}{\rho(4.2K)} \tag{1.11}$$

RRR values serves as a convenient measure of the purity of the metal. High-purity niobium has higher RRR values; the theoretical limit is 35000 and is determined by scattering of electrons by lattice vibration.

In a sputtered cavity, the grain size and the purity of the thin film are such that the mean free path l is very small (10-100 nm) nevertheless the Q_0 of such a cavity is twice that of a cavity made from high RRR bulk niobium.

The mean free path in the niobium is strongly influenced by interstitial impurities like oxygen, nitrogen and carbon, as well as residual tantalum impurities.

The critical parameter for Superconducting Radio Frequency (SRF) cavities is the surface resistance R_s, and is where the complex physics comes into play. For normal-conducting copper cavities operating near room temperature, R_s is simply determined by the empirically measured bulk electrical conductivity σ by

$$R_s = \sqrt{\frac{\omega\mu_0}{2\sigma}} \tag{1.12}$$

For Type II superconductors in RF fields, R_s can be viewed as the sum of the superconducting BCS resistance and temperature-independent residual resistances,

$$R_s = R_{BCS} + R_{res} \tag{1.13}$$

The BCS resistance derives from BCS theory, which proposed by Bardeen, Cooper, and Schrieffer. The theory describes superconductivity as a microscopic effect caused by a condensation of pairs of electrons into a boson-like state [5] [6] [7].

They assumed that electrons below T_c begin to condense to pairs of electrons, the so called Cooper pairs. The two electrons in a pair have opposite momentum and spin. They experience an attractive force mediated via quantized lattice vibrations called phonons. This bound state of the two electrons is energetically favorable. As the overall spin of these two paired electrons is zero, many of these pairs can co-exist coherently, just like other bosons. The coherence length describes the distance over which the electrons are correlated.

It is given by:

$$\xi = \frac{h v_F}{\Delta} \tag{1.14}$$

where:

v_F denotes the velocity of the electrons near the Fermi level

2Δ is the energy necessary to break up a Cooper pair.

Typical values for the coherence length in niobium are around 39 nm. If one interprets the coherence length as the size of a Cooper pair, one immediately sees that it spans over many lattice constants.

Within the BCS theory the energy gap can be calculated:

$$\Delta = 1.76 k_B T \tag{1.15}$$

One way to view the nature of the BCS RF resistance is that the superconducting cooper pairs, which have zero resistance for DC current, have finite mass and momentum which has to alternate sinusoidal for the AC currents of RF fields, thus giving rise to a small energy loss. The BCS resistance for niobium can be approximated when the temperature is less than half of niobium's superconducting critical temperature, $T < T_c/2$, by:

$$R_{BCS} = 2\times 10^{-13}\left(\frac{f}{1.5\times 10^{9}}\right)\frac{e^{-17.67/T}}{T} \tag{1.16}$$

T_c=9.3 K for niobium, so that this approximation is valid for T<4.65 K.

The superconductor's residual resistance arises from several sources, such as random material defects, hydrides that can form on the surface due to hot chemistry and slow cool-down, and others that are yet to be identified. One of the quantifiable residual resistance contributions is due to an external magnetic field pinning magnetic fluxons in a Type II superconductor. The pinned fluxon cores create small normal-conducting regions in the niobium that can be summed to estimate their net resistance.

For niobium, the magnetic field contribution to R_s can be approximated by:

$$R_{res} = R_H = 9.49 \times 10^{-12} H_{ext} \sqrt{f} \tag{1.17}$$

where:

H_{ext} is any external magnetic field

The residual resistance is usually dominated by lattice imperfections, chemical impurities, adsorbed gases and trapped magnetic field. Well prepared niobium surfaces show a residual resistance of a few nΩ

Using the above approximations for a niobium a SRF cavity at 1.8K, 1.3GHz, and assuming a magnetic field of 10mOe (0.8A/m), the surface resistance components would be:

R_{BCS}=4.55nΩ

R_{res}=R_H=3.42nΩ

R_s=7.97nΩ.

If for this cavity G=270Ω then the ideal quality factor would be Q_o=3.4×10^{10} [8] [9] [10] [11].

1.3 Thin film

A thin film is a layer of material ranging from fractions of a nanometer (monolayer) to several micrometers in thickness. It is a thin layer of material which is located on a bulk material. The benefit of incorporating thin films with some other material is that it allows combining the properties of the bulk material with the properties of the thin film.

The act of applying a thin film to a surface is thin-film deposition, any technique for depositing a thin film of material onto a substrate or onto previously deposited layers. If the thickness of a thin film should be less than 1 micrometer, it is understandable that a process that produces such a thin film with desirable properties is not straightforward. The atoms of the target have to be extracted and be transported from the target to the substrate. When the atoms reach the substrate they will have to condense on the substrate in order to form a film. Clever techniques have been developed which allow this process to be controlled, to some extent. The film will grow under conditions which can be set, and eventually result in a desired growth.

Physical deposition uses mechanical or thermodynamic means to produce a thin film of solid. The material to be deposited is placed in an energetic, entropic environment, so that particles of material escape its surface. Facing this source is a cooler surface which draws energy from these particles as they arrive, allowing them to form a solid layer. The whole system is kept in a vacuum deposition chamber, to allow the particles to travel as freely as possible. Since particles tend to follow a straight path, films deposited by physical means are commonly directional, rather than conformal.

Sputtering involves a target, which is a solid source of material that will be a component of the resulting film. The target along with the substrate, onto which the film will grow, are kept in a vacuum chamber to reduce contamination in the film from other constituents present in the surrounding atmosphere, and in some cases to increase the mean free path of the particle transportation, so that particles extracted from the target are allowed to travel to the substrate with very few collisions. The

extraction of particles is a rather complicated process with several steps involved. But simply explained it can be achieved by applying a negative voltage to the target to attract positive ions from a working gas inside the chamber. The working gas is usually argon, which does not react with the film. Thus by using an inert working gas contamination can be avoided despite the fact that the base pressure usually is high enough (in the order of 1-100mTorr) to expose the substrate to a significant number of impinging atoms. In fact, if air would be present instead of argon, a monolayer would form in about 10^{-6}s at room temperature. When the ions are attracted onto the target they will be neutralized and the released energy ideally causes an atom at the surface of the target to escape in a direction towards the substrate. This is a sputtering event, and the target atom can now be transported towards the substrate, eventually condense on the surface and start building a thin film [14].

2 Magnetron Sputtering

2.1 Fundamentals

Sputtering is a process whereby atoms are ejected from a solid target material due to bombardment of the target by energetic particles. It is commonly used for thin-film deposition, etching and analytical techniques [15] [16]. Sputtering deposition is a physical vapor deposition (PVD) method of depositing thin films.

A material-bombarding particle, like a single atom, ion or molecule with a relatively high potential energy can give rise to the ejection of secondary electrons or other phenomenon, like breaking or rearranging chemical bonds. If the kinetic energy of the bombarding particles exceeds the binding energy of the atoms, atoms of the lattice are pushed into new position; surface migration of the atoms and surface damage can arise [17] [18].

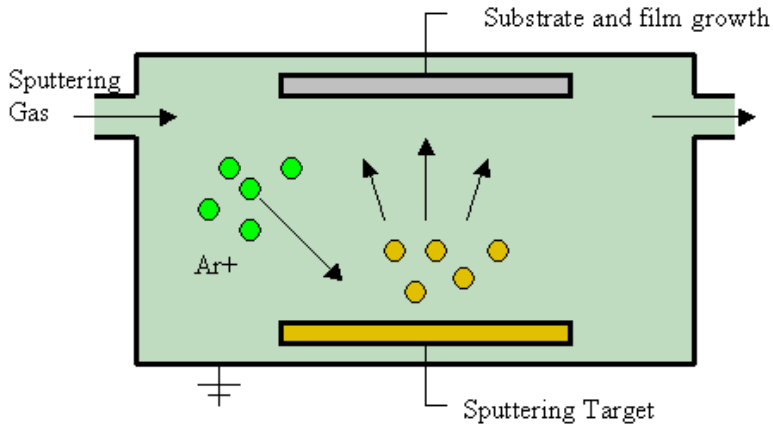

Figure 2.1: Physical vapor deposition

Sputtering is a technique by which atoms and ions of argon or other gases from plasma bombard a target thereby eject atoms off the target. These material atoms travel to a substrate where they are deposited and form a thin film. Diode sputtering is the simplest configuration and consists of two electrodes placed in a vacuum chamber.

Sputtering is always associated with temporary or permanent lattice damage and surface migration of atoms. For this reason sputtering is often considered as an

inconvenience as it causes erosion of the electrodes, damage to active surface layers in thermionic low work-function cathodes, undesirable deposits on walls and observation windows etc. One can say that sputtering is responsible for limiting the useful life of a lot of devices including old electronic vacuum triodes (television) valves or even gas lasers.

If a DC voltage is applied between two electrodes spaced at some distance d apart in a gas at low pressure, a small current will flow. This is caused by small number of ions and electrons, which are always present in a gas due ionization, by cosmic radiation. On their way from the cathode to the anode, the electrons make a fixed number of ionizing collisions per unit length. Each ionization process produces further electrons, while resulting ions are accelerated toward the cathode. If the applied voltage is enough, ions striking the cathode can eject secondary electrons from its surface. Emission ratio of secondary electrons of most materials is of the order of 0.1, so several ions are needed to bombard a given area of the cathode in order to release secondary electrons. If the power supplied is not high enough, the bombardment is concentrated near the edges of the cathode. When the power supplied increases, the bombardment covers the entire cathode surface and a constant current is achieved.

The two processes of ionization by electron impact and secondary emission of electrons by ions, control the current I in the system, described by the equation

$$I = \frac{I_0 e^{\alpha d}}{1-\gamma(e^{\alpha d}-1)} \tag{2.1}$$

where:

I_0 is the primary electron current generated at the cathode by the external source

α is the number of ions per unit length produced by the electrons

d is the spacing between the electrodes

γ is the number of secondary electrons emitted per incident ion.

According to *Townsend criteria*, $\gamma(e^{\alpha d}-1)=1$ if the voltage between the electrodes is raised, the current becomes infinite. It is said that gas breakdown has occurred; the glow discharge burns self-sustained, as the number of secondary electrons produced at the cathode is sufficient to maintain the discharge. Breakdown voltage is a function of the product of pressure *p* and electrode distance *d*.

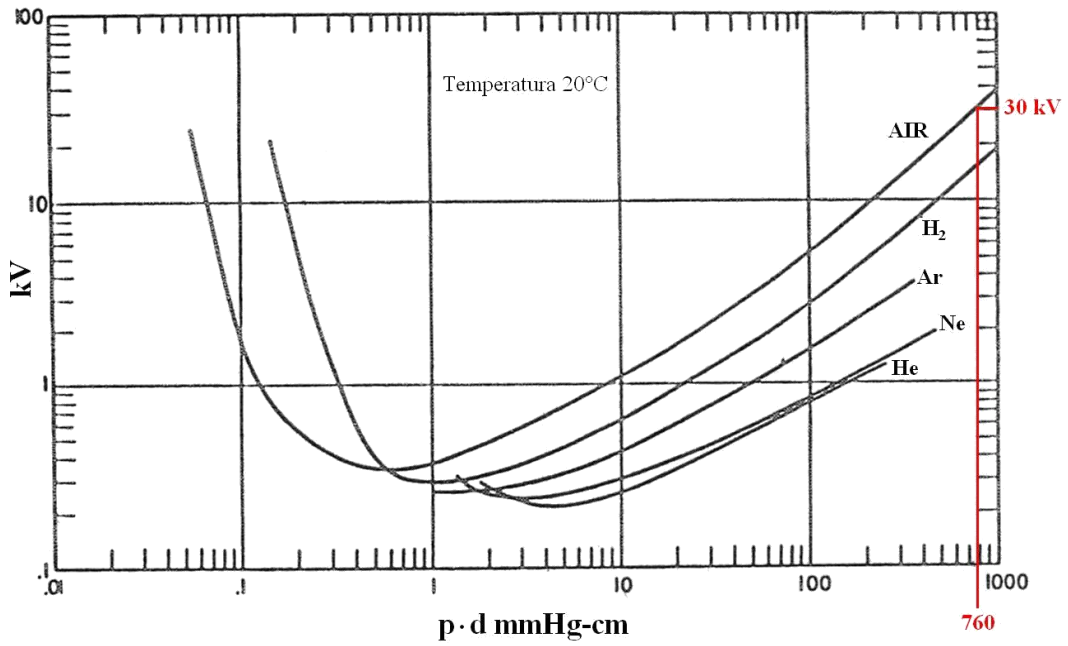

Figure 2.2 Paschen's law

Distribution of potential, field, space charge and current density in a glow discharge are visually seen as region of varied luminosity. From a cross sectional view of a glow discharge we see as of primary interest the region marked as *Crookes Dark Space* (also called *Cathode Dark Space*). In this region, the positive ions have accumulated and have formed the space charge. Its thickness is approximately the mean distance travelled by an electron from the cathode before it makes an ionizing collision. Usually this distance is 5-10 times longer than the electronic mean free path *l*. The electron energies are over the maximum excitation potential which is insufficient to ionize gas molecules, so that no visible light is emitted.

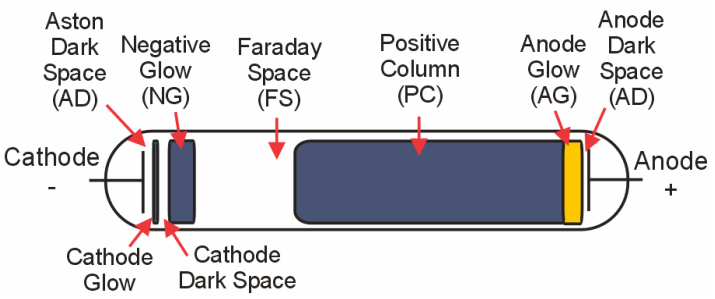

Figure 2.3: Cross sectional view of a glow discharge.

Electrons that leave the cathode with energy of the order of 1eV are accelerated to sufficient ionizing energies in a region called *Aston's dark space*. The luminous region closest to the cathode is the *cathode glow* where the electrons reach energies corresponding to the ionization potential. When the electrons reach the edge of the *negative glow*, they begin to produce significant numbers of ion-electron pairs. The number of slow electrons has become very large. The energy they posses are enough to cause only excitation and can't produce new ionization. Excitations caused by slow electrons are the reason of the appearance of the negative glow. In Faraday dark space the electrons have insufficient energy to cause either ionization or excitation, consequently is a dark space. *Faraday dark space* and *the positive column* are nearly field-free regions with nearly equivalent numbers of ions and electrons. For glow discharges applied as sputtering sources, the positive column and the Faraday dark space usually do not exist, as the electrode separation needs to be small and the anode is located in the negative glow.

2.2 DC magnetron sputtering (DCMS)

The common way of generating plasma for material processing by magnetron sputtering is to use two metal electrodes: a cathode and an anode (usually the grounded chamber walls) enclosed in an evacuated vacuum chamber. In order to generate the plasma a source of power is needed, such as a direct current (DC) power supply.

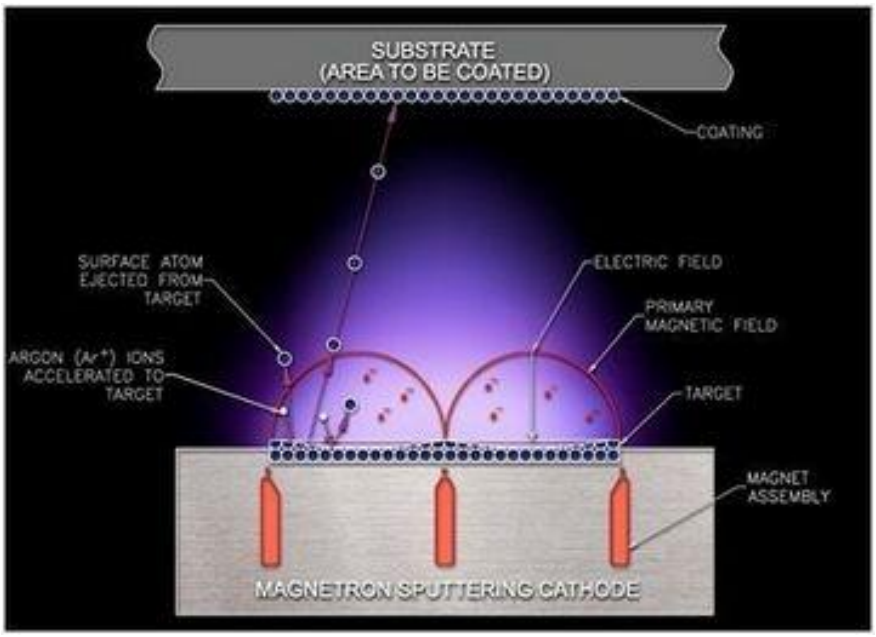

Figure 2.4 Magnetron sputtering

The reason for the magnetron being excellent in confining the plasma is the magnetic field configuration combined with an electric field, such as the one generated by applying an electrical voltage. One example is where the magnets are placed with one pole positioned at the central axis of a circular magnetron, and the second pole placed in a ring configuration around the outer edge.

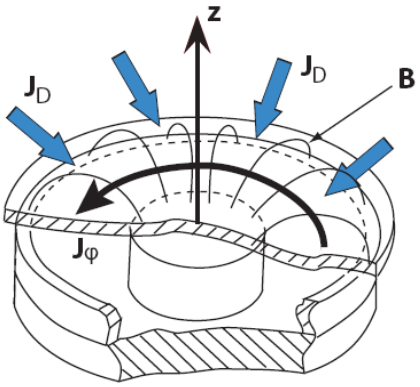

Figure 2.5 The circular planar magnetron cathode

For an effective sputtering, primary electrons must be used effectively to make sufficient ionization collisions in the vicinity of the cathode. The efficiency of the available electrons can be increased if the plasma is confined by a magnetic field parallel to the cathode surface. A general rule for the shape of the magnetic field is:

Magnetic field must bore from the cathode and die onto the target. That means that a plasma confinement is achieved, while magnetic and/or electrostatic mirrors trap the electrons. The magnetic field traps and forces electrons to describe helical paths around the lines of magnetic force.

The magnets are arranged in such a way that they create a closed drift region; electrons are trapped, and rely on collisions to escape. By trapping the electrons in this way, the probability for ionization is increased by orders of magnitudes. Ions are also subjected to the same force, but due to their larger mass, the Larmor radius often exceeds the dimensions of the plasma.

Larmor radius:

$$r_g = \frac{V_E}{\omega_c} = \frac{m_e}{e}\left(\frac{V_E}{B}\right) = 3.37\frac{\sqrt{W}}{B} \qquad (2.2)$$

where:

V_E is the drift speed of electrons

W is the energy associated with the electron motion perpendicular to the field

Although in general one says that the ions are not directly confined, they are so indirectly by trapping the electrons, to keep the quasi neutrality of the plasma. The trapping of electrons and ions creates dense plasma, which in turn leads to an increased ion bombardment of the target, giving higher sputtering rates and, therefore, higher deposition rates at the substrate. The electron confinement also allows for a magnetron to be operated at much lower voltages compared to basic sputtering (~ 500 V instead of 2-3 kV) and be used at lower pressures (typically mTorr region). This is an advantage since less material is lost to the chamber wall and back to the target through scattering in the discharge gas. The shape of the magnetic field efficiently erodes the target where the magnetic field lines are parallel to the target surface; a so-called race-track is created.

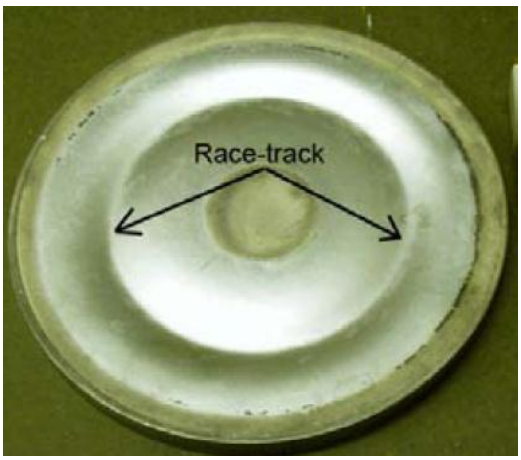

Figure 2.6The sputtering race-track

The ways to confine electrons on the target are making electrons deflecting into closed paths or by magnetostatic bottle or by electrostatic mirror.

As the electrons can move freely along the field lines, end losses are possible. The problem is eliminated installing reflecting surface wings (mirrors) maintained at the cathode potential or by causing the magnetic field lines intersect that cathode. In order to complete the electrical circuit, the low energy electrons must be removed from the trap and migrate to the anode. It is believed that plasma oscillations assist in this process. Anode placement, size and design are of an important role and should take into account the poor mobility of the low-energy electrons. Proper anode placement and design can greatly reduce spurious electrical activity.

A spool formed from a cylindrical barrel and two wings is called a cylindrical post magnetron cathode. In a relatively uniform magnetic field, a uniform intense plasma will form along the barrel and will extend outward a distance *W*. The smallest wing size *W* should be at least three times larger that the gyro radius of the primary electrons emitted from the cathode.

The minimum wing size:

$$W = \frac{10\sqrt{V}}{B} \tag{2.3}$$

where:

B: magnetron field strength

V: operation voltage

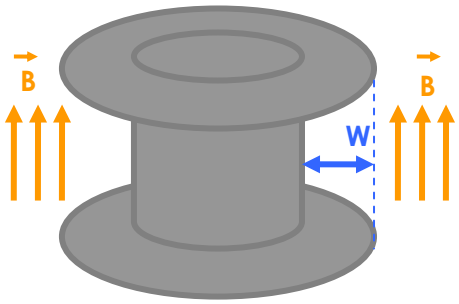

Figure 2.7 The cylindrical post magnetron cathode

The current voltage characteristic of a magnetron reveals a wealth of information on the processes of ionization in a discharge plasma, the higher the efficiency of ionization and lower the voltage required to achieve a given cathodic current density, i.e. it is necessary to use less electrical power for obtain a fixed deposition rate. There are two possible models that attempt to describe the dependence of the current function of the voltage setting.

The first model provides the following behavior:

$$I = aV^n \tag{2.4}$$

where:

n (between 5 and 10) is greater the more effective

It is the confinement by the magnetic field.

The second model provides a rather characteristic of the type:

$$I = a(V - V_0)^2 \tag{2.5}$$

where:

V_0 is the potential for ignition of the plasma.

2.3 Film growth

Plasma is a state of matter similar to gas in which a certain portion of the particles are ionized. The basic premise is that heating a gas dissociates its molecular bonds, rendering it into its constituent atoms. Further heating leads to ionization (a loss of electrons), turning it into plasma: containing charged particles, positive ions

and negative electrons [19].

Plasmas are used in a number of ways in the field of thin film production and surface modification. Consider an object inserted into plasma. If the object is subjected to a negative electrical potential compared to the plasma body, the positively charged ions in the plasma will be accelerated towards the object. At the object surface a number of processes and combinations of them can occur.

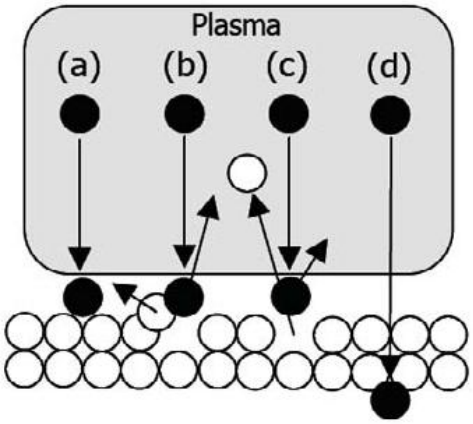

Figure 2.8 Effects of bombarding ions or neutral atoms onto a surface
(a) adsorption (b) displacement (momentum transfer),
(c) removal of surface atom (sputtering or etching), (d) ion implantation.

The cascade of ionizing collisions will ultimately result in a large current causing the gas to break down, and eventually the discharge becomes self-sustaining, meaning that enough secondary electrons are generated to produce the required amount of ions to regenerate the same number of electrons. The gas begins to glow and there is a sharp voltage drop, and we are now in the normal glow regime [20]. With increasing power the current density will eventually be rather evenly distributed over the entire cathode surface. If one increases the power even further the abnormal discharge regime will be reached. Here, the ion bombardment already covers the whole cathode surface and the increased power results in both an increase in voltage as well as current density. The resulting charge carrier density (plasma density) is found in the range from 10^{15} m^{-3} to 10^{19} m^{-3}. Here is where plasma processing, such as sputtering and etching, takes place [21]. Increasing the current density even further results in

thermionic emission of electrons at the cathode. The voltage drops sharply, but the current density is very high. This is an arc discharge and is the regime used for cathodic arc deposition [22].

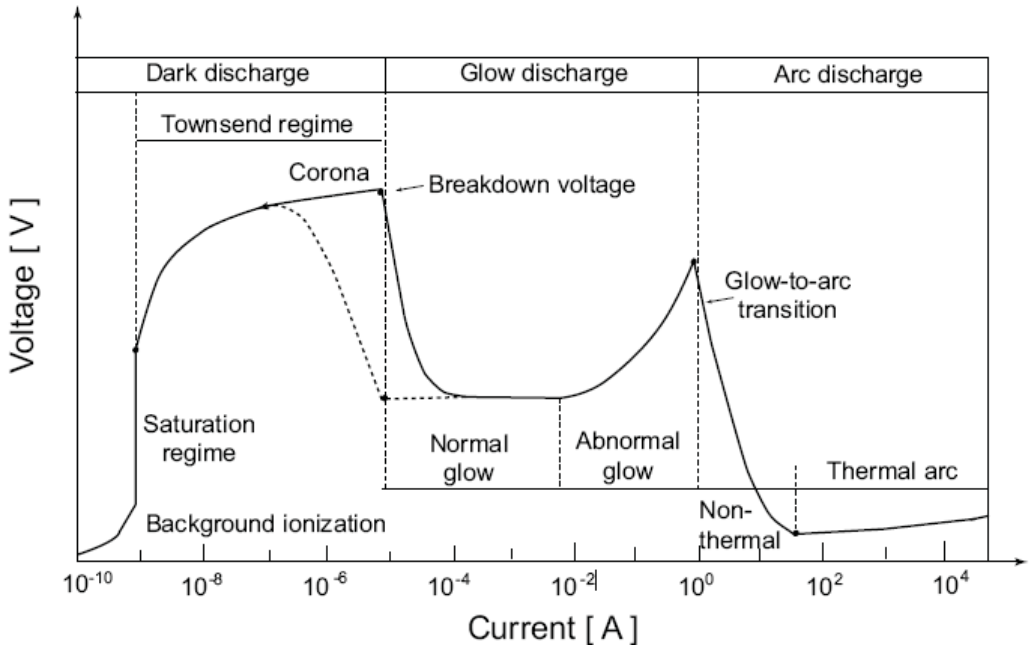

Figure 2.9 Plasma discharge regimes

The most common plasma-based thin film growth techniques are sputtering and cathodic arc evaporation, and various combinations and versions of them. Sputtering alone typically produces low-density, weakly ionized plasma, whereas cathodic arc produces dense highly ionized plasma, but a major drawback are the microdroplets, which reduce the quality of the films when not filtered out.

In a sputtering process a minimum deposition-rate to carry out the deposition does not exist, instead in the evaporation process it does. During sputtering process deposition of the film material is done atom by atom on the substrate. One of the advantages of the sputtering versus thermal evaporation is that sputtering yield of different materials do not vary that much. Thus refractory materials, which require high temperature and low vapor pressure, sputter almost as readily as any other material. Anyway, the sedentary nature of sputtered refractory materials appears at the point of deposition. The diffusion from the random point of impingement onto energetically favorable sites is restricted form the low mobility of the sputtered

material. The microstructure and properties of coating deposited is, however, influenced a lot from the plasma sputtering environment, which can be manipulated [23]. Without any modification of the plasma environment one can obtain primitive growth structures that are not strongly interbonded.

The deposition of thermally evaporated metals in the form of tapered grains was determined by Movchan and Demchishin [24] to occur at temperatures below about 1/3 of the respective melting temperature. Thornton adapted their zone diagram for metal coating deposited by plasma sputtering just adding a second axis for sputtering gas pressure.

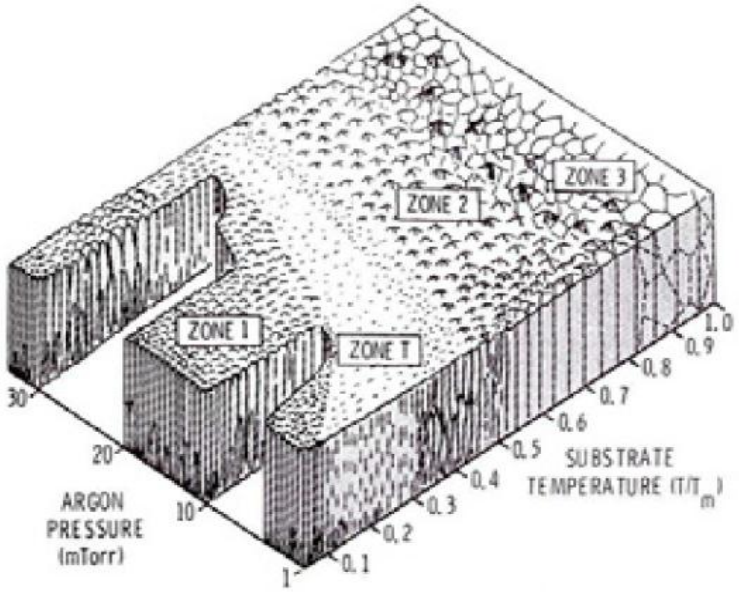

Figure 2.10: Sputtering structural zone model

The diagram indicates that the microstructure properties of the sputtered film depend not only on the substrate temperature, but also on the gas pressure.

A positive bias applied between target and substrates promotes ion bombardment of the growing film. If the film is given a negative potential with respect to the plasma, the resulting technique is referred to as bias sputtering. In this way films are subjected to a certain amount of resputtering that causes the desorption and breakup by ion bombardment of the surface adsorbed species; whether or not this will occur depends on the relative strengths of the metal-to-impurity and the metal-to-metal bonds [25].

The impurity fraction:

$$f_i = \frac{\alpha_i N_i}{\alpha_i N_i + R} \tag{2.4}$$

where:

N_i is the number of atoms of species *i* bombarding unit area of film in unit time during deposition

α_i is the effective sticking coefficient of the species *i* during deposition

R is the deposition rate of the film

Considering the bias:

$$f_i = \frac{\alpha_i N_i - \beta}{\alpha_i N_i - \beta + R} \tag{2.5}$$

where:

β is a function of the bias current due to impurities ions

From early morphology studies, the film structure is highly correlated with the deposition rate and the adatom surface mobility [26, 27]. By increasing the incident atom energy and incident flux, we can expect increased substrate temperature right at the surface, and higher adatom surface mobility, which leads to the larger grain size. Based on this and the findings in [28], Schucan et. al., have tried to use Ar/He mixture as working gas to increase the argon ionization efficiency during sputtering [29]. Unfortunately rare gas trapping reduces the grain size and affects the grain growth. The investigation of the rare gas trapping of Ar, Ke and Xe is reported in [30]. Sputtering film technique has the following drawbacks:

- the working gas is trapped in the film; it may cause intrinsic defects inside of the grain. And the impurities of the working gas are not good for the thin film.
- the deposition energy is low, which does not help to avoid columnar grains.

3 HIPIMS

3.1 Fundamental

High Power Impulse Magnetron Sputtering (HIPIMS), also known as High Power Pulsed Magnetron Sputtering (HPPMS) is a method for physical vapor deposition of thin films which is based on magnetron sputter deposition. HIPIMS utilizes extremely high power densities of the order of $kWcm^{-2}$ in short pulses (impulses) of tens of microseconds at low duty cycle (on/off time ratio) of < 10%. A distinguishing feature of HIPIMS is its high degree of ionization of the sputtered metal and high rate of molecular gas dissociation.

HIPIMS was first reported in 1999 by Kouznetsov *et al*, [31-37] who also patented the technique together with the company Chemfilt R&D. The basis of the technique is to increase the plasma density in front of a sputtering source, and, thereby, decreasing the mean ionization distance for the sputtered particles. The increase in plasma density is simply achieved by applying a high electrical power. The electrical power applied to the target surface has to be high enough so electron densities of the order of 10^{19}–10^{20} m^{-3} are reached in the vicinity of the sputtering source. In reality this corresponds to electrical power of the order of $kWcm^{-2}$ on the target surface, which is too much to be run in constant mode with conventional target cooling. The solution to this problem is to apply the high power in pulses with a low duty factor. The duty factor is the ratio of the pulse on time and the cycle time. The target cooling is limited by the average power rather than the peak power, and by applying the power in pulses the average power can be kept at where the cooling is sufficient. The discharge is uniformly distributed over the target surface. This is necessary to avoid the formation of microdroplets.

The peak power that must be delivered to the target is typically of the order of $kWcm^{-2}$, meaning that the power supply must be able to deliver a peak electrical power in the range 10kW-5MW, depending on the target size. The pulse is then repeated with such a frequency that the average power is kept low.

HIPIMS plasma is generated by a glow discharge where the discharge current density can reach up to 6 Acm^{-2}, whilst the discharge voltage is maintained at several hundred volts. The discharge is homogeneously distributed across the surface of the cathode of the chamber. HIPIMS generates high density plasma of the order of 10^{13} ions cm^{-3} containing high fractions of target metal ions. The main ionization mechanism is electron impact, which is balanced by charge exchange and diffusion. The ionization rates depend on the plasma density.

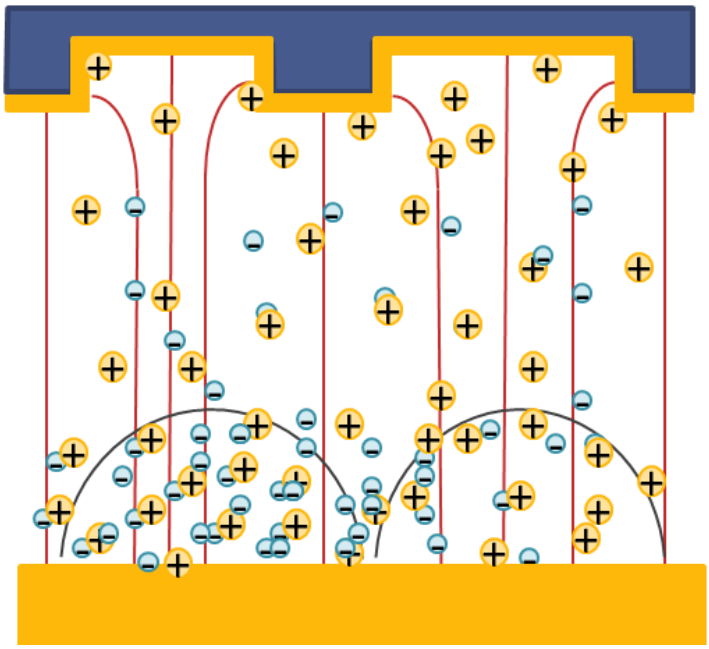

Figure 3.1 Schematic view of the HIPIMS system

The ionization degree of the metal vapor is a strong function of the peak current density of the discharge. At high current densities, sputtered ions with charge 2+ and higher up to 5+ for V can be generated. The appearance of target ions with charge states higher than 1+ is responsible for a potential secondary electron emission process that has a higher emission coefficient than the kinetic secondary emission found in conventional glow discharges. The establishment of a potential secondary electron emission may enhance the current of the discharge.

HIPIMS is typically operated in short pulse (impulse) mode with a low duty cycle in order to avoid overheating of the target and other system components. In

every pulse the discharge goes through several stages: electrical breakdown, gas plasma, metal plasma, steady state, which may be reached if the metal plasma is dense enough to effectively dominate over the gas plasma

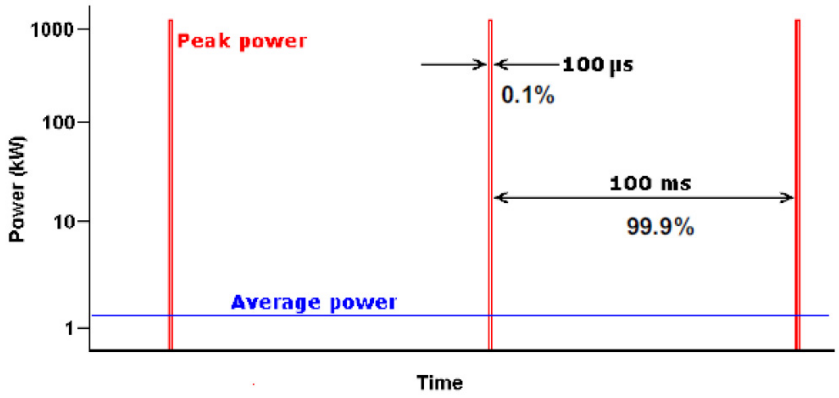

Figure 3.2 HIPIMS cycle

The discharge that maintains HIPIMS is a high-current glow discharge, which is transient or quasistationary. Each pulse remains a glow up to a critical duration after which it transits to an arc discharge. If pulse length is kept below the critical, the discharge operates in a stable fashion infinitely.

3.2 Electrical parameters

A common way to define the strength of the pulse is to define the pulse energy. The pulse energy can be obtained in several ways. One is to measure the voltage and current and multiply the two traces. The result is the discharge power as function of time. The integration of this curve then gives the pulse energy. Alternatively one can measure the voltage or current separately, and with knowledge of the capacitance of the capacitor bank, the stored energy can be obtained. A typical value of the pulse energy is $50 mJcm^{-2}$.

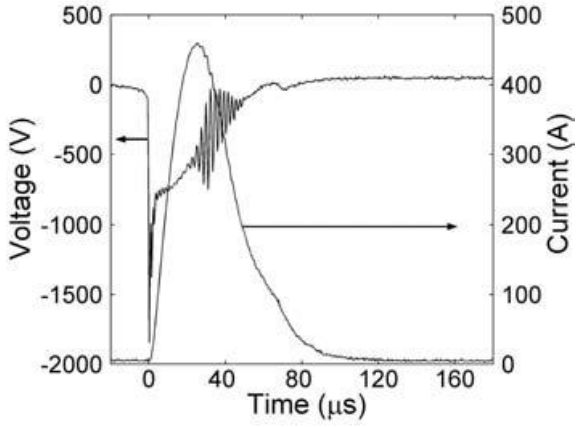

Figure 3.3 The current and voltage curve of HIPIMS

The electrical pulses are generally generated by discharging a capacitor bank via a semiconductor-based switch. The capacitors are charged by a power supply, and discharged in a repetitive manner. The size of the capacitor bank is typically 1-50μF, depending on the size of the target.

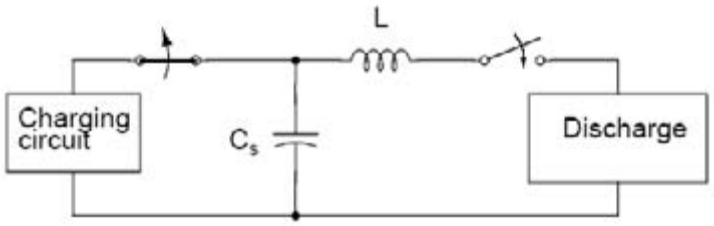

Figure 3.4 HIPIMS power supply

There is also an inductance on the output. The size of the inductance is typically 20-50μH [38, 39, and 40]. The inductance prevents that the current increase is too steep, and damages the circuitry.

3.3 Properties

The main advantage is the control over energy and direction of the deposition material. In some sense, HIPIMS can be seen as a method that combines the advantages of conventional magnetron sputtering and arc evaporation. It produces

highly ionized droplet free plasma. As mentioned previously, today there are a number of plasma based processes that effectively ionize the deposition material. The main advantage of HIPIMS compared to these methods is the simplicity. Any existing magnetron-based deposition system can directly, or with little reconstruction, be turned into an IPVD system. This is an important feature for large-scale industrial applications. In principle all one needs is a HIPIMS power supply. The highly ionized conditions in HIPIMS can be used in a number of areas to improve the properties and performance of thin films.

The plasma conditions in HIPIMS can be used for growth of films using a bombardment of ions of the target material itself, which often results in dense, droplet free films. Dekoven *et al* [41] found that C films grown by HIPIMS had significantly higher density (>35%) compared to films grown by conventional magnetron sputtering. Sproul *et al* [42] demonstrated the possibility to produce oxide films with control over the optical parameters. Alami *et al* [43] showed that Ti-Si-C films grown by HIPIMS exhibited an enhanced microstructure. Films grown with HIPIMS on tilted surfaces showed improved quality [44].

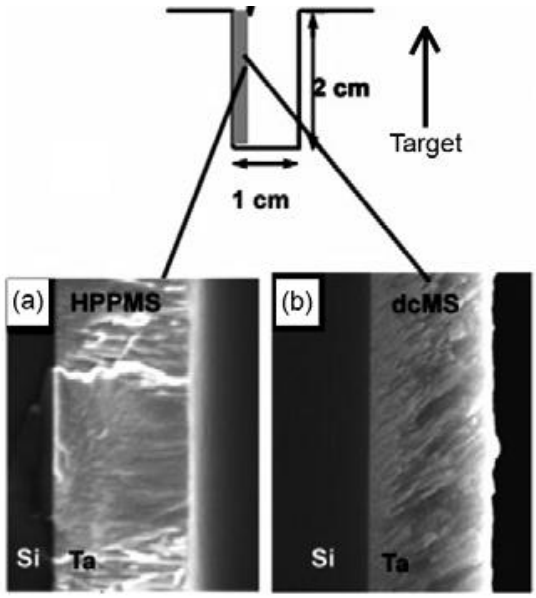

Figure 3.5 Comparison between two Ta films grown by HIPIMS and conventional magnetron sputtering

You can see two Ta films grown under similar conditions on 90° tilted Si Substrates in respect to the target surface. The film shown in (a) is a film grown by HIPIMS while (b) is grown with conventional sputtering. The film produced by HIPIMS exhibited a dense microstructure, with less columnar structure. No tilting of the columns was observed.

From the point of view of accelerator techniques, coatings produced with HIPIMS are highly interesting as it has been proven that the film properties are enhanced. One can expect better adhesion [45], a better (normal) conductivity, less defects in the crystal, as well as dense and smooth films [46, 47]. This results from the fact that the target material is partly ionized such that the ions will reach the target with a higher energy and, in case of an applied bias voltage to the substrate, always perpendicular to the surface. The result is a homogeneous coating even on non-flat surfaces.

Previous investigations of DCMS Nb films on Cu cavities have shown that the RF performance is strongly depending on the film quality [48]. Thus the use of HIPIMS for the production Nb thin film cavities can possibly push the limitations towards a better performance.

The main problems with the current version of HIPIMS are reduction of deposition rate and the transition to an arc discharge. The deposition rate for the HIPIMS discharge is expected to be in the range 30-80 % compared to a conventional magnetron discharge, with the same average power. Bugaev *et al* [49] reported factor a reduction with a factor 2 for Cu and Ti sputtering. For reactive sputtering from a Ti target (TiO2 films) a reduction of 4-7 times has been observed [50]. One explanation for the reduction in deposition rate is that some of the material that is ionized is attracted back to the cathode. In the presence of a magnetic field, as in a magnetron discharge, not all potential drops occurs over the sheath region, but a fraction of the applied voltage will penetrate the bulk plasma and create a plasma potential gradient. If a sputtered atom is ionized within this region it needs to have enough kinetic energy to overcome this potential in order to reach the substrate. If not, the sputtered atom is drawn back to the target, and causes so-called self-sputtering. In this case the ion is no

longer available for deposition, and the rate drops. A plot of the deposition rate for HIPIMS compared to conventional sputtering versus the ratio between the self-sputtering yield, and the Ar yield (that is the dominant mechanism in conventional sputtering) is evidence that self-sputtering is an important mechanism in HIPIMS.

The other problem with HIPIMS is the arcing tendency on the cathode surface. There are mainly two types of arcs. Heavy arcs and light arcs. The light arc is minor problem, since it does not produce large number of microdroplets, as the heavy arc does. The light arc can be seen as a little spark on the target surface that does not extend further into the bulk plasma. The heavy arc can however be a serious problem. Heavy arcs can sometimes be observed as extended plasma columns going from the cathode into the bulk plasma. The arc locally heats the target, and microdroplets can be ejected.

3.4 Applications

HIPIMS is currently taking the first steps towards industrial applications. The unique features of the discharge should be well suited for a number of application areas.

One of them is surface pre-treatment. The highly ionized and metallic plasma is well suited for combined etching and ion implantation. These might involve adhesion enhancer for coatings on various tools (etching) and adhesion layer for coatings on various substrates

Another is film growth. The current version of HIPIMS, with the reduced deposition rate, should be applied to products where the increase in production cost is small in comparison to the gain in film quality. These can be areas where really thin films are desired or for coatings on expensive products, for example high-tech electronics.

A few suggested application areas are:

1) Metallization in general

2) Interconnects in IC structures

3) Protective overcoats on hard disks and read-write heads

4) Deposition onto complex shaped objects

5) Coatings on medical products

6) Conducting & transparent electrodes in flat panel displays touch panel displays, solar cells, etc.

7) Al coatings in numerous applications

8) Optical coatings: anti-reflective and anti-static coatings, optical filters

9) Wear-corrosion-resistive coatings: cutting tools, tribological applications, etc.

10) Ag mirrors

11) Coatings on plastics

4 Experiment system

4.1 Introduction

The experiment system is consisted of the following parts:

1 The vacuum system. High to ultra-high vacuum removes the obstruction of air, allowing particle beams to deposit.

2 The control system. Including control box and baking box, manages and commands the behavior of the experiment system.

3 The cooling system. Including water cooling and air cooling, transfers the thermal energy out of the experiment system.

4 The Ar supply system. Argon is preferred for the sputter coating; it is the cheapest noble gases, since it is a byproduct of the production of liquid oxygen and liquid nitrogen from a cryogenic air separation unit, both of which are used on a large industrial scale. Also, argon is the most plentiful since it has the highest concentration in the atmosphere. The bulk of argon applications arise simply because it is inert and relatively cheap.

5 The magnetron coil and support system. The magnetron coil is used to produce the external magnetic field, for not limiting the Curie temperature permanent magnets and to simplify the structure of the maximum post magnetron and minimize the problems related to high temperatures that have occurred during the preliminary tests. Also, all the system is standing upon the coil.

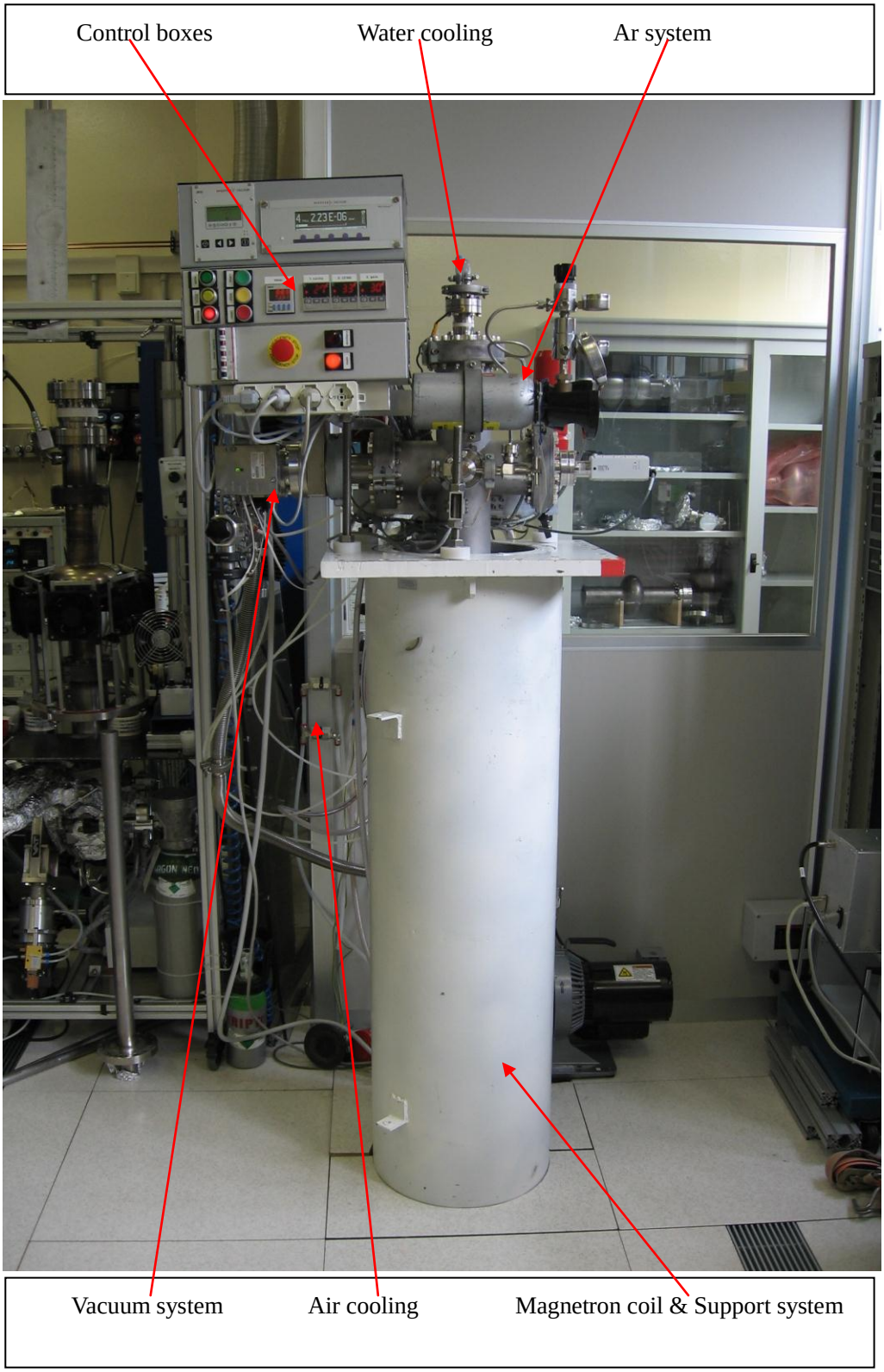

Figure 4.1 The experiment system

4.2 Vacuum system

The vacuum is consisted of primary pump, turbo molecular pump, valves, vacuum chamber, gauges, etc.

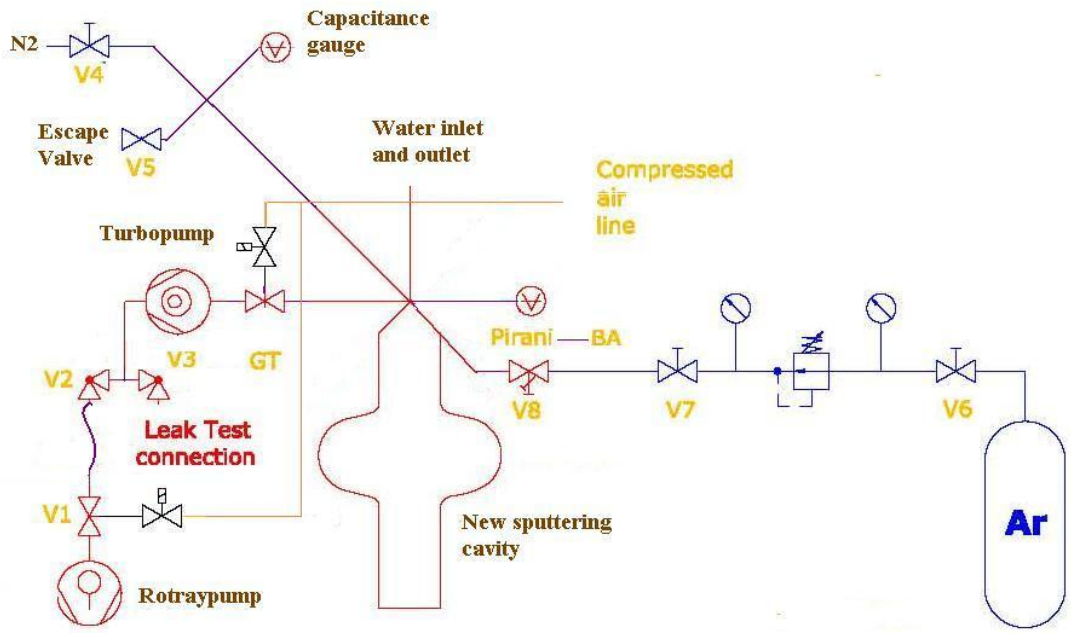

Figure 4.2 The vacuum system

The primary pump is mounted a pump Varian Scroll reaching a limit of 10^{-2} mbar vacuum. The choice of a dry pump was dictated by the need to have an extremely clean. The pump is equipped with an electro-pneumatic valve (V1) that opens and closes when the pump with it's off, or in case of power failure.

Figure 4.3 Varian Scroll

After the pump there is a second electro-pneumatic valve (V2) used to isolate the scroll from the system during the leak test, which is done by opening the manual valve angle of VAT (V3). Below is a Pfeiffer turbo molecular pump capacity of 60 l/s. The turbo molecular pump is separated by a gate valve Varian (GT).

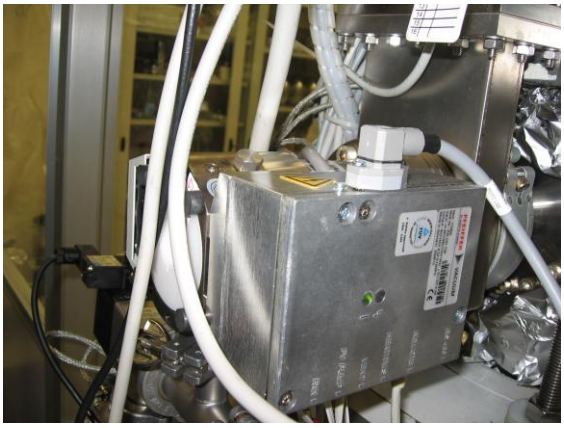

Figure 4.4 Pfeiffer turbo molecular pump

CF63 to 6-way cross flange CF100 and CF35 are set to cross the cavity in the upper flange and the cathode. Always comes to cross process gas (argon purity 99.9999%) and the line for venting gas (nitrogen).

Argon is "stored" in a small cylinder from a fixed to the system through a ring of steel. The connection between the cylinder and the line uses a system Cajon, followed by an all-metal angle valve (V7) and a valve Varian all-metal precision dosing valves of VAT (V8).

Figure 4.5 The argon supply line

Also the central chamber are connected the two pressure gauges vacuum system. Also for this system has opted for a full-range and a capacitive are used during the depositions. Here are the full specifications of the two gauges: Full Range (BA-PI) Pfeiffer (range of pressures measured 10^{3}-10^{-10} mbar) and Capacitive CMR264 Pfeiffer (range of pressures measured 10^{3}-10^{-4} mbar).

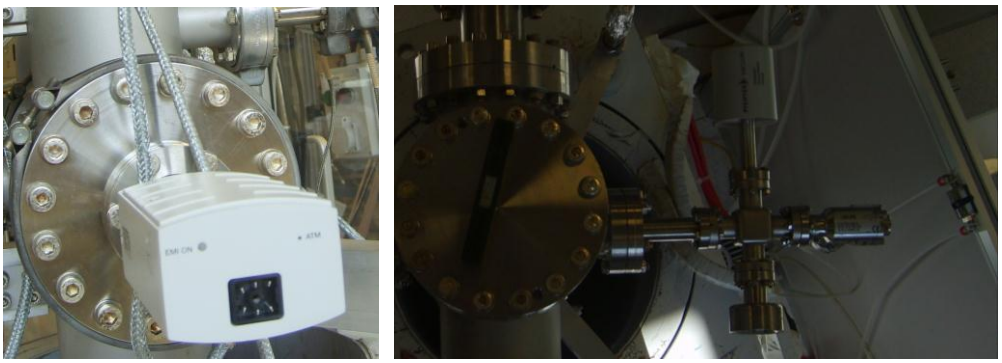

Figure 4.6 Full Range (BA-PI) Pfeiffer and Capacitive CMR264 Pfeiffer

Anchored to the system there are three check boxes that contain the turbo molecular pump controller, the maxi gauge Pfeifer for measuring the vacuum level, and allow the pump drive scroll, the opening and closing the gate's Drive and control system for baking.

Figure 4.7 The control boxes

4.3 Control system

The system of baking is needed to make the chamber vacuum achieving 10^{-9}-10^{-10} mbar, Treatment of baking in the system provides for a minimum period of 30hours to reach those results in terms of vacuum level.

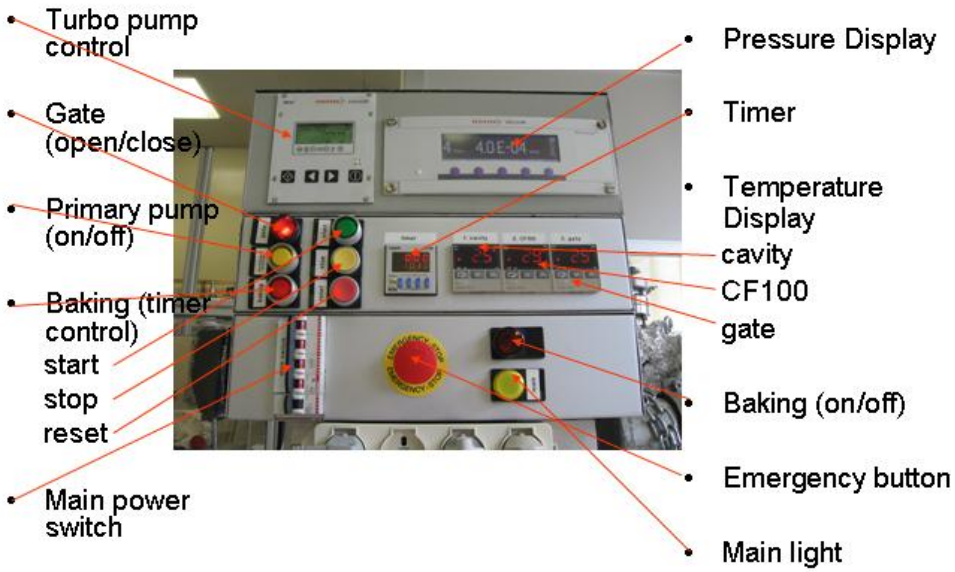

Figure 4.8 The control system

The need for a compact system has prevented the use of an additional rack on which to mount the electrical box control (pumps, gauges and gate), and the heavy units UHV BAKING CONTROL for controlling the baking process, which is normally mounted on the vacuum systems of LNL. The applicant has therefore had to implement a system that contained miniaturized electric control:

a) A system for monitoring the process of baking

b) Control for switching on and off the scroll pump

c) Control the opening and closing the gate

d) Controller pump turbo molecular

e) Controller of Gauges (Multigauge Pfeiffer)

f) Power to all electrical equipment of the system (eg, turbo molecular pump, heating rings, etc.).

It was decided to use two boxes of size 390x160x100 mm 390x230x145 mm and a third (containing Maxi gauge Pfeiffer and the Pfeiffer turbo molecular pump controller) mounted on an aluminum arm anchored by screws, a fin welded to vacuum chamber.

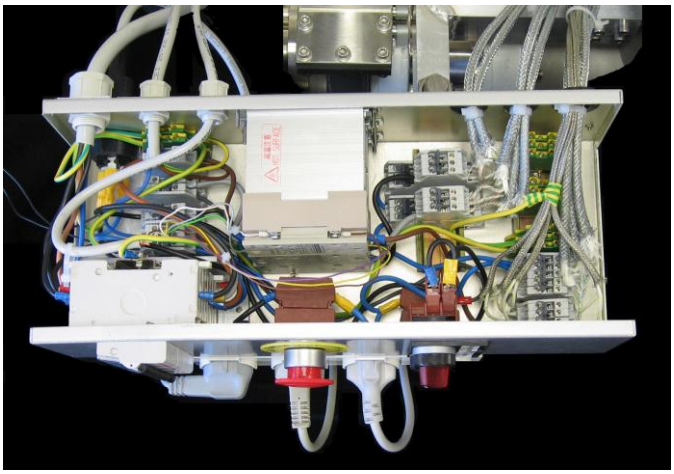

Figure 4.9 The control box A

The switch, the three solid state relays, the emergency button and the selector switch on and off the power strip to which are fed turbomolecular pump, pump controller and maxigauge. On the right are also the terminals on which the power cables coming heating rings, already divided into three distinct areas. The cooling fan is fixed to the top cover and therefore not visible.

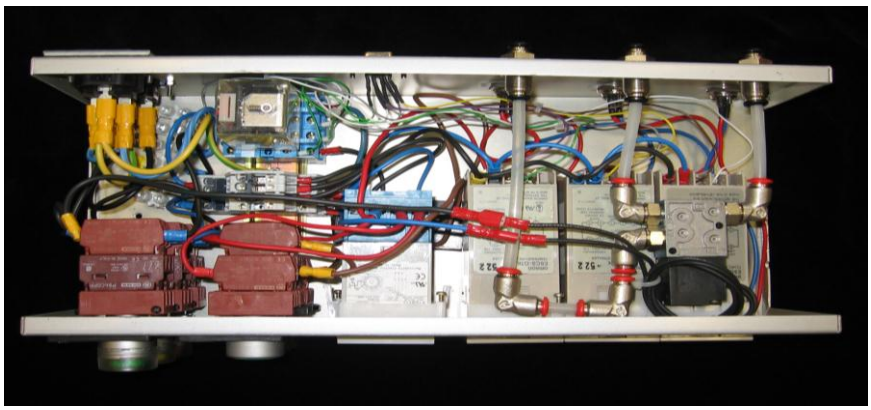

Figure 4.10 The control box B

From left: the buttons, relay, timer, three controllers of temperature and above them the solenoid valve to control the gate.

4.4 The cathode

The most important and delicate whole system is the cathode. It must be secured to the flange CF100 top of the system and measuring exactly 684 mm from the tooth of the flange at the center of the post magnetron, the latter fact is positioned perfectly in the center of the cavity. Throughout this length there should be nothing to discover potential, if not the same post magnetron. Another critical point of this component is the high operating temperatures (about 2000 °C post on the magnetron). It understands how the tolerances required and construction constraints that make the rather complicated to implement.

Figure 4.11 The cathode

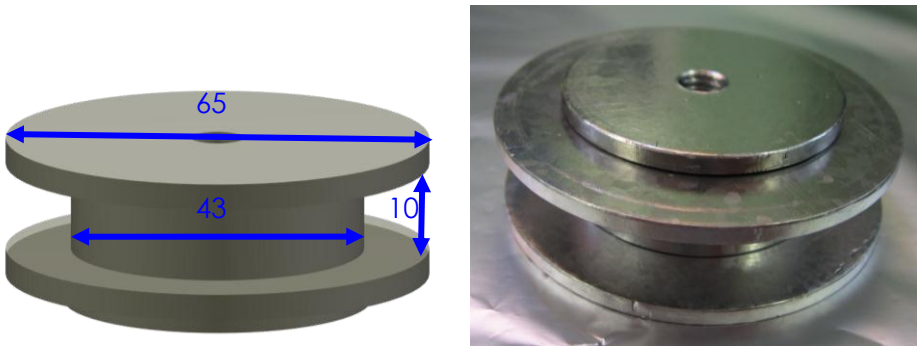

Figure 4.12 The post magnetron

One problem lies in the cavity temperature reached during the sputtering. After just over five to ten minutes is required to stop the process because the outside of the cavity reaches 200 ° C, despite a cool place with a continuous flow of compressed air at 7 bar.

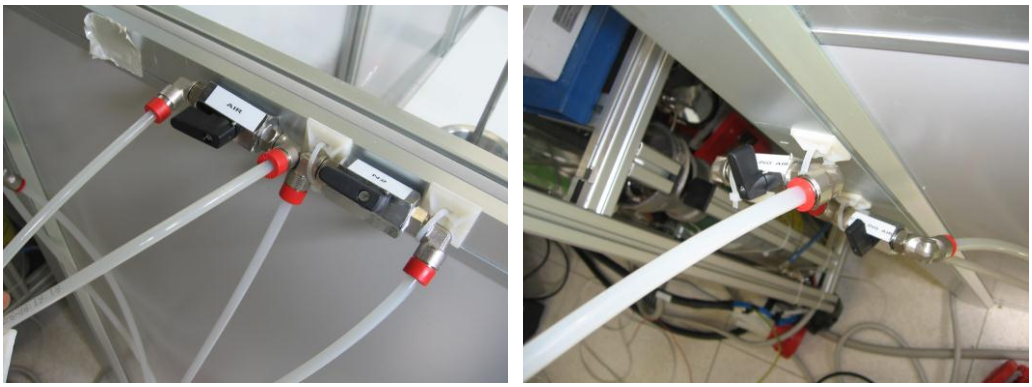

Figure 4.13 The cooling air system

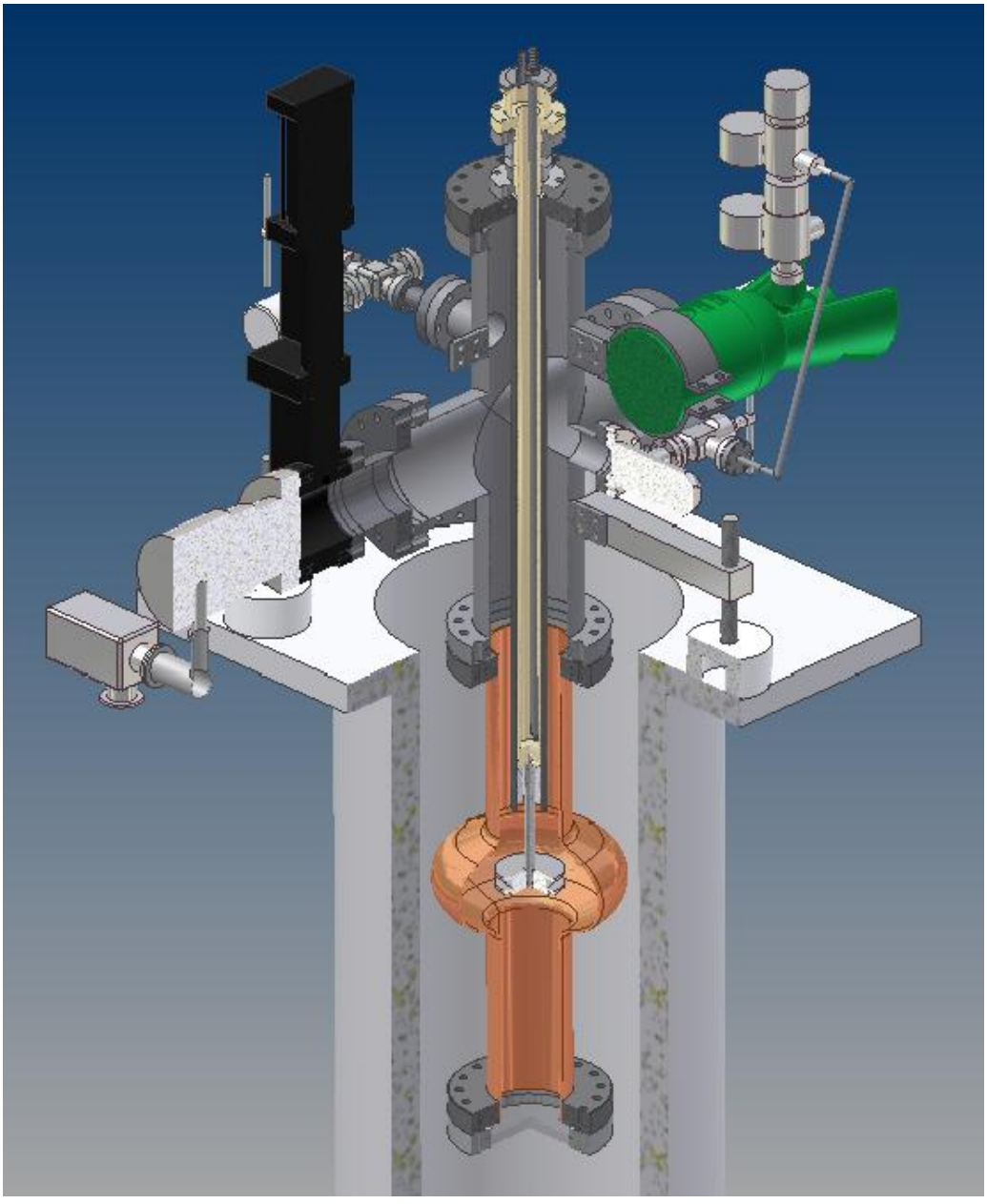

Figure 4.14 The deposition system (sectional drawing)

4.5 The power supply

To make a deposition in this system requires two power supplies, one for the cathode and one to feed the coil. The cathode power supply is TRUMF HÜTTINGHER Electronic TruPlasma Highpulse: DC Unit, 4002 High Impulse Power, Impedance Matching Circuit. The coil is fed by Hitachi DT - NP3 300; a TIG capable of delivering up to 300 A.

Figure 4.15 TruPlasma Highpulse units

Figure 4.16 Hitachi DT - NP3 300

4.6 The coil

Given the high coil height, the cavity is not at the center of the same when the system is located. This is because the system is designed to be used with a second coil, smaller but capable of delivering a more intense magnetic field (1000 Gauss) used only for the last deposition, it has previously been used for other experiments. The magnetic field is still uniform along the cavity with both coils. The coil is powered with a current of 295 A using the supplied Hitachi and under these conditions provides a magnetic field along the longitudinal axis of about 450 Gauss.

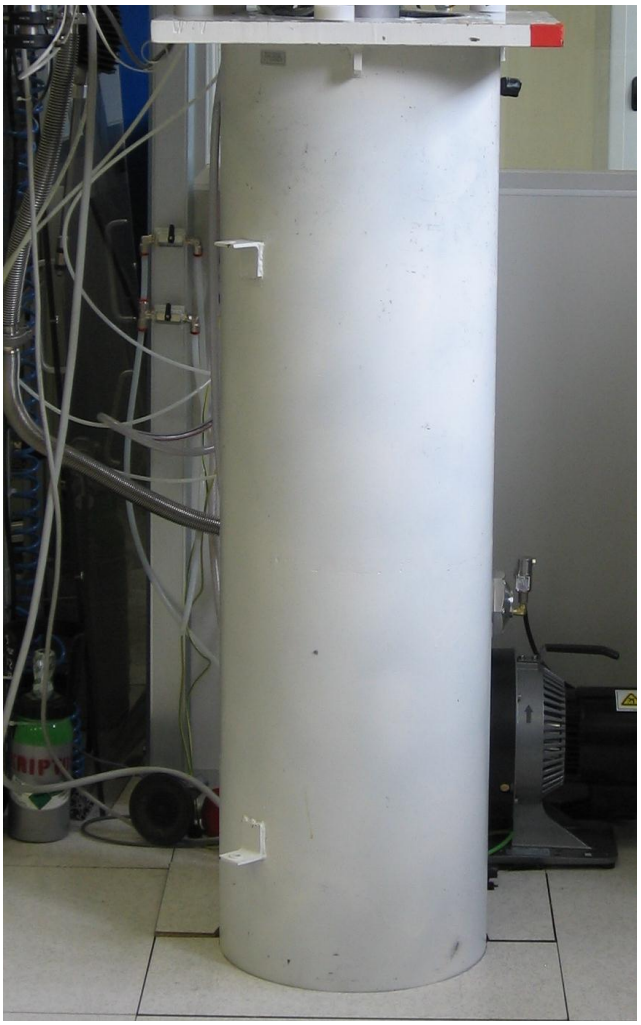

Figure 4.16 The coil

5 Experimental details

5.1 Ultrasonic Cleaning

An ultrasonic cleaner is a cleaning device that uses ultrasounds (usually from 20–400 kHz) and an appropriate cleaning solvent (sometimes ordinary tap water) to clean delicate items. The ultrasound can be used with only water but solvent is advised; it enhances the effect of a solvent appropriate for the item to be cleaned and the soiling.

Before sputtering, the quartz glasses as substrates should be cleaned.

The procedure is:

1st, clean glasses with soap water for 20 minutes;

2nd, clean glasses with water for 20 minutes;

3rd, dry glasses with ethanol and put them into a bottle with ethanol.

Figure 5.1 Ultrasonic cleaner BRANSON 5510

Before sputtering, also the cavity should be cleaned.

The procedure is:

1st, clean cavity with soap water for 60 minutes;

2nd, clean cavity with water for 30 minutes;

3rd, dry cavity with ethanol and air, and then cover them with aluminum.

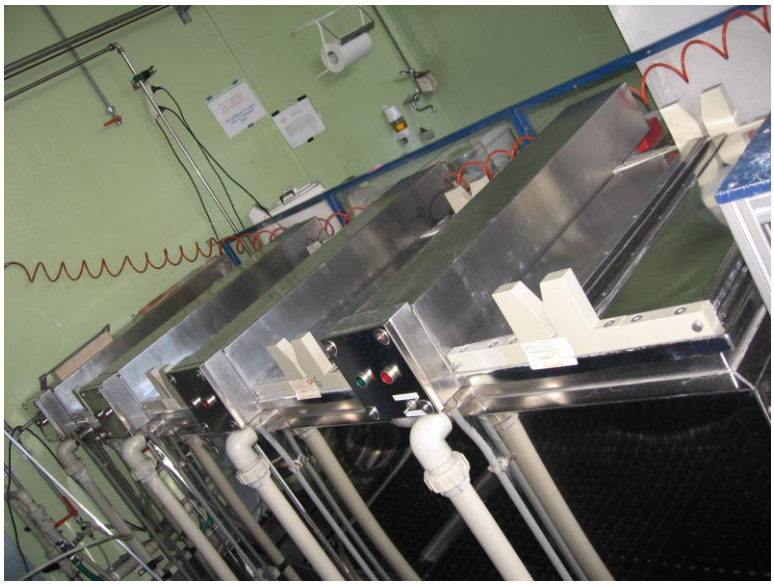

Figure 5.2 The ultrasonic cleaning bathes

5.2 Assembling samples and cavity

After cleaning the samples, they need to be assembled and fixed by bolts, nuts and washers on the two holders. Then, putting on ethanol and drying them by compressed pure N_2 gas.

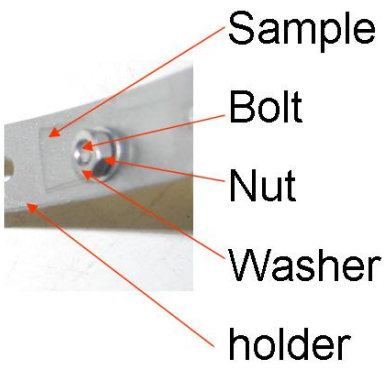

Figure 5.3 Assembling samples

Figure 5.4 Two sample holders

Then, assembling cavity:

1st, assembly holders with samples into the cavity;

2nd, assembly cavity onto vacuum tube, pay attention to the cathode;

3rd, assembly heaters onto cavity cover the cavity with aluminum;

4th, put them onto coil bucket and fix them.

Figure 5.5 Assembling sample holders on cavity

5.3 Pumping and baking

After assembling, pumping the vacuum system and baking it to have the UHV.

1st, start primary pump and open the gate valve;

2nd, start turbo pump and the pressure go down to 10^{-5} mbar;

3rd, when the pressure goes down to 10^{-6} mbar, start baking.

Before baking, cover the system with aluminum;

Then, set the temperatures of baking: for cavity: 250℃ for CF100: 180℃ and for Gate: 120℃;

After, set the time of baking, it should be more than 30 hours;

Finally, turn on the button of baking, start baking;

Don't forget to stick the pay attention note to the system to prevent others hurting by the high temperature.

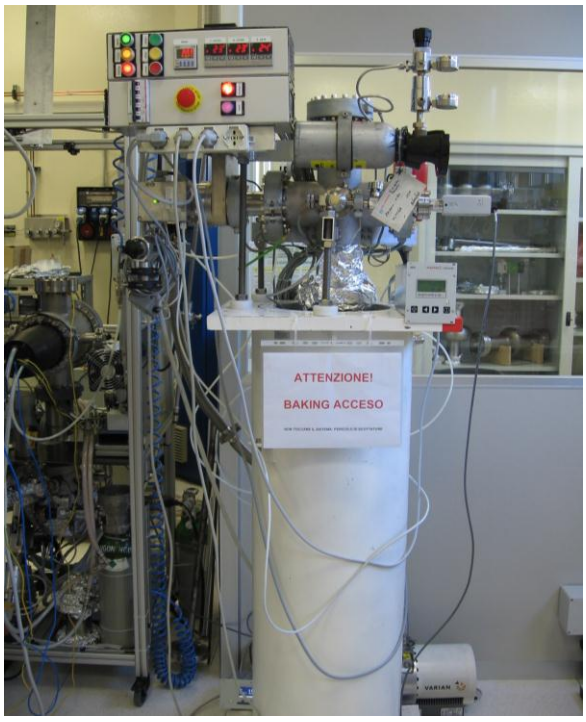

Figure 5.6 Pumping and baking

After baking the pressure should be lower than 8×10^{-9} mbar; then, close the gate, stop the turbo pump, remove all aluminum and remove the three heaters on cavity; restart pump, the pressure should be also lower than 8×10^{-9} mbar.

5.4 Sputtering

When the pressure is lower than 8×10^{-9} mbar, the sputtering can be started. Before sputtering, some preparation should be done.

To connect cooling water and check if there is water in the pipes. For the heat when sputtering is very high, to protect the target, water cooling is needed.

There are two water pipes: water in and water out. Water in the pipes is used as the heat transmitter.

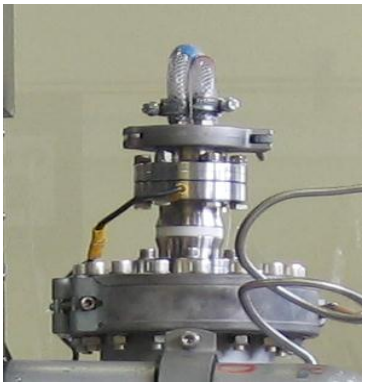

Figure 5.7 Water in and water out on the top of the system

To connect coil power supply and connect HIPIMS power supply. The cathode connects to negative voltage and the cavity connects to ground.

Open Ar bottle to put Ar into the system for sputtering.

When sputtering, the temperature of the cavity is very high, so open the air cooling to cool the outer of the cavity.

Connect to PC control. Link the PC to HIPIMS power supply to control it. After connecting success, set parameter of HIPIMS in pc, using the software PVD power.

Meanwhile, count the time and take notes when sputtering.

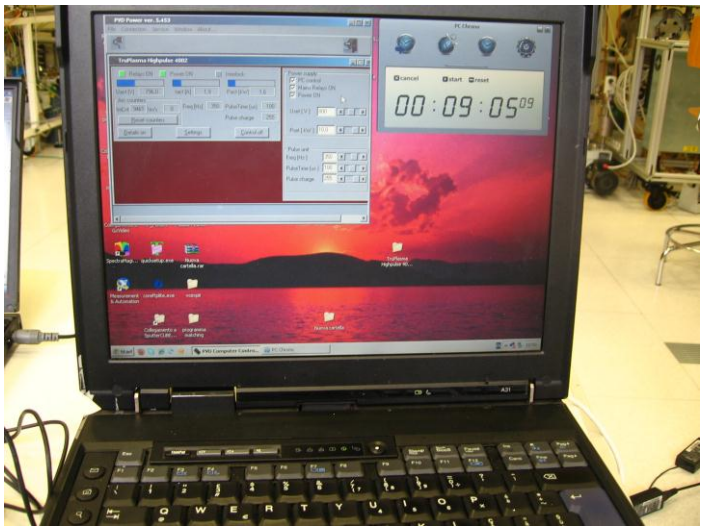

Figure 5.8 The interface of HIPIMS PC control

When sputtering, turn the flow valve to control the pressure.

Figure 5.9 The Ar pressure control

When the temperature reaches 190 degree stop, wait for temperature going down to 60 degree restart sputtering. The total time of sputtering should be more than 1 hour to reach a thickness more than 1 μ m. .

5.5 Disassembling

After sputtering, wait for the temperature of the cathode going down; Close the gate, stop the pumps and vent the vacuum system; Disassembly the cavity and remove all samples; Number all the samples and put the samples into a box.

Figure 5.10 The samples in sample box

6 The characterization techniques

6.1 Measurement of the thickness

To check the thickness of deposited films, a Veeco profile meter model Dektat 8 has been used. The instrument consists of a bit of sliding on the sample to be measured by pressing it with a constant force (set at 10 mg in this analysis).

Figure 6.1 Dektat 8 and PC control

The roughness of the surface is reflected in a vertical movement of the tip and cantilever in which it is attached. The cantilever is connected to a capacitor, and the vertical movement of the tip results in a specific capacitance of this capacitor, the system converts a profile on the screen of the PC. The sample to be measured must be flat and hard enough not to be scratched from the tip, also must have an area not filed in such a way as to measure the height difference between this and the area covered by the film. All samples produced by the observed characteristics, the attachment to the quartz sample holder by screw, nut and washer, produce a masking effect on the sample and

thus allow the analysis to the profile meter. The scan is performed from the area that had not been filed with the movie, to prevent an error in the selection of scan length, to bring out the tip from the sample, causing serious damage.

The Scan parameters are:

Scan Type: Standard Scan

Stylus: Radius 5 µ m

Length: 2500 µ m

Duration: 20sec

Force: 10mg

Measurement Range: 65500nm

Profile: Hills & Valleys

The measurement is performed by running samples on 6 different scans lengths of 2.5 mm, at 3 different points of the step masked by the deposition of the semicircle, and 2 for each deposition. For each scan gives the film thickness, obtained as an average value over a length of 2.5 mm of niobium deposited. On the average 6 values you get for the average thickness of the film of niobium, for a given sample with its standard deviation.

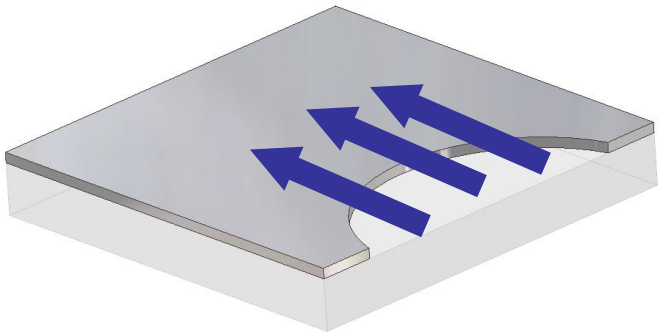

Figure 6.2 Location of the scans of the samples analyzed

6.2 Measurement of the reticular parameters

X-ray scattering techniques are a family of non-destructive analytical techniques which reveal information about the crystallographic structure, chemical composition, and physical properties of materials and thin films. These techniques are based on observing the scattered intensity of an X-ray beam hitting a sample as a function of incident and scattered angle, polarization, and wavelength or energy.

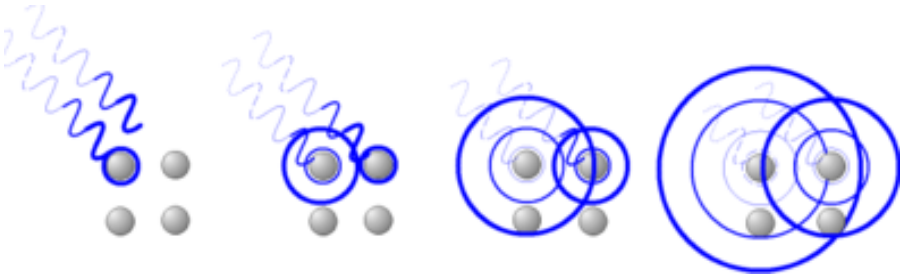

Figure 6.3 X-rays interact with the atoms in a crystal

Through the X-ray diffraction we aim was to study the changes implemented on the crystal structure of niobium as a function of format used for the deposition of thin films. Specifically, it was verified the change of crystalline grain size and the presence of residual stresses in the film, determined by calculating the change in the interplanar distance through Bragg's law:

$$2d_{(h\ k)l}\sin\theta = n\lambda \tag{6.1}$$

where：

λ is the wavelength of incident wave,

d is the spacing between the planes in the atomic lattice

θ is the angle between the incident ray and the scattering planes.

The lattice parameter:

$$a = \sqrt{h^2 + k^2 + l^2}\cdot d_{hkl} \tag{6.2}$$

The grain size:

$$D = \frac{0.9\lambda}{\cos(\theta)\cdot\Delta(2\theta)} \tag{6.3}$$

2 θ	Relative intensity	Miller indices (hkl)
38.51	100	1 1 0
55.59	16	2 0 0
69.65	20	2 1 1
82.53	5	2 2 0
95.00	4	3 1 0
107.73	1	2 2 2
121.45	4	3 2 1
137.69	<1	4 0 0

Table 6.1 diffraction peaks of film of niobium

The test apparatus to identify and characterize the films we used a Bragg diffract meter Philips Xpert-Pro powder. The X-ray beam is generated by a tube to the Cu and the detector is a proportional counter consists of a cylindrical chamber which contains a mixture of argon and methane. These detectors measure the current generated by ionization of gas atoms by interaction with X-rays that pass through it.

Figure 6.4 Philips X'Pert diffract meter

For the characterization of powders and bulk samples used is the standard configuration of the diffract meter with both arms moving. For the characterization of thin films, on the arm of the detector was mounted a collimator for analysis of thin films from 0.18°, it consists of a series of parallel plates that restrict the viewing angle of the incoming beam to 0.18°. The scan in this case is performed with grazing incident beam to the sample, while the arm is moved on which is mounted on X-ray detector.

With a quick scan type identifies the exact location of the peak (110) of niobium for the test sample, while the film to that in the massive material and stress-free at 2θ=38,503° may be shifted slightly due to phenomena of stress or errors induced by imperfect flatness of the sample or the sample holder assembly is not exactly horizontal. Source and detector are positioned so that the sample is in a position of reflection peak for (110), will not be changed for the duration of the measurement.

6.3 Measurement of the superconducting properties

The superconducting theory is described in chapter one. The behavior of a superconducting material is essentially characterized by two basic parameters: The Residual Resistivity Ratio (RRR) and the critical temperature (T_c).

The Residual Resistivity Ratio (RRR) is calculated by:

$$RRR = \frac{R(300K)}{R(10K)} \tag{6.4}$$

Since the residual strength is essentially determined by the amount of impurities present in the sample, RRR provides an estimate of the immediate quality of the material: the higher the more the sample is pure, that acts as a "good" superconductor. It is also a dimensionless parameter which has the advantage of being able to leave by the geometric dimensions that remain constant with changes in temperature and therefore cancel out.

The critical temperature is the temperature at which the sample makes the superconducting transition, the point below which the DC electrical resistance falls, ideally to a value below the limits of instrument sensitivity and thus can be taken as nil. The transition temperature $T_c \pm \Delta T_c$ is calculated after obtaining the whole resistance curve, using the formula:

$$T_c = \frac{T_{(90\%)} + T_{(10\%)}}{2}$$
$$\Delta T_C = \frac{T_{(90\%)} - T_{(10\%)}}{2} \tag{6.5}$$

where:

T (90%) is the temperature at which the resistance has a value equal to 90% of that before the transition

T (10%) as the temperature at which the resistance is 10% above that of the transition

The resistance measurement is made using the method voltage-amperage with four points: the standard four contacts are welded, the outer two inject a sinusoidal current, oscillating at a frequency set, while the two interior capable of measuring the voltage drop. Applying Ohm's law R =V/I gives the resistance of the sample.

The current inversion is to avoid systematic errors due to contact resistance: if there is a constant offset voltage V_0, the measured voltage V_m, will be made by the actual voltage V across the contacts as the offset value and therefore calculating the resistance of the sample will be wrong. Reversing the sign of the current only affects the voltage measured by contact and not on the offset voltage, thus mediating the measure on the two values V_1, V_2 obtained with current of opposite sign should be eliminated or at least limit the offset:

$$V_m = \frac{V_1 + V_2}{2} = \frac{(V + V_0) - (V_0 - V)}{2} \approx V \tag{6.6}$$

The procedure is:

1st Put sample into the four points' measurement container.

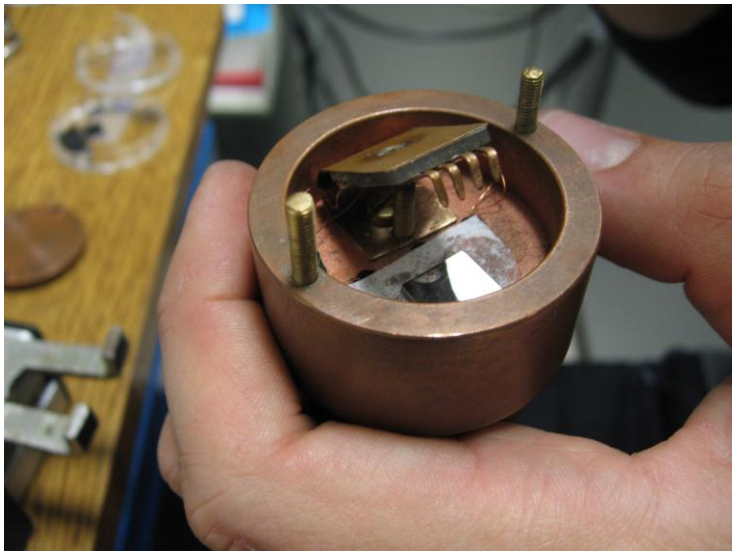

Figure 6.5 The four points measurement container

2nd Put the probe into the liquid helium pot.

Figure 6.6 The liquid helium pot

3rd Start measuring

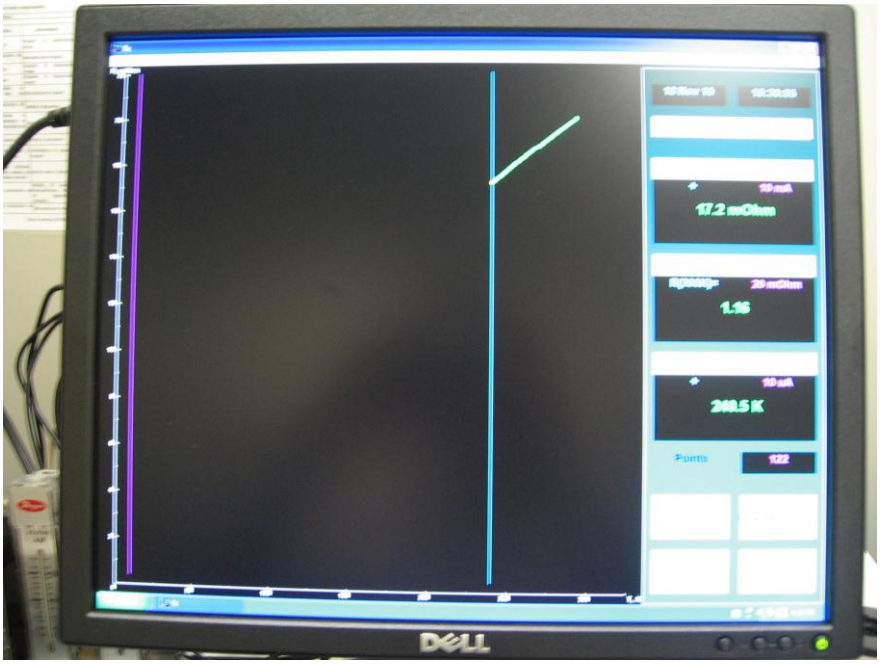

Figure 6.7 The measuring interface

After measuring, use software Origin to deal with the data. Then calculate RRR T_c and ΔT_c.

7 Summary of results

7.1 Deposition conditions

Base pressure: 4 10^{-9} mbar*

Sputtering pressure: 8 10^{-3} mbar (Argon)*

Magnetic field: 400 Gauss

Run	Uset (V)	Freq (Hz)	Pulse Time (μs)	Pset (kW)	Pulse Charge	Magnetron Current (A)	Total Time (min)
Run0	*320*	-	-	-	*1.0*	*1.0*	*60*
Run1	600	200	200	10	255	1.4	60
Run2	600	300	50	10	255	0.4	10
Run3	600	500	50	10	255	0.8	60
Run4	600	500	100	10	255	1.2	75
Run5	600	500	150	10	255	1.7	60
Run6	600	500	200	10	255	2.0	60
Run7	800	350	100	10	255	1.6	60
Run8	800	500	50	10	255	1.1	80
Run9	800	500	100	10	255	1.4	60
Run10	800	500	150	10	255	2.1	60
Run11	800	500	200	10	255	2.2	60
Run12	1000	200	50	10	255	1.0	60
Run13	1000	300	50	10	255	1.2	60
Run14	1000	400	50	10	255	1.4	60
Run15	1000	500	50	10	255	1.6	60
Run16	1000	500	200	10	255	2.2	60

Table 7.1 Deposition conditions of HIPIMS

Run 0 is a test run obtain in magnetron sputtering technique with a DC power supply. All the other runs are obtain with HIPIMS deposition.

For each run, there are more than seven parameters to control. Here is just the main parameters list. The most important parameters are the Uset (V) stand for the

voltage added to cathode, the Frequency (Hz) and the Pulse time (μs). The following analysis is mainly based on these three parameters.

For each run, eight samples are fixed at different positions on sample holders inside the cavity, to have a global view of the deposition of HIPIMS. The position of the samples are shown in figure 7.1(a) and. figure 7.1(b).

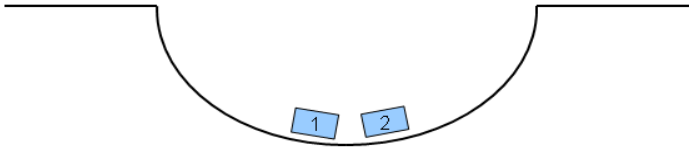

Figure 7.1(a) The position of sample A1 and A2

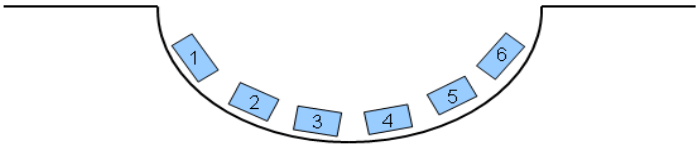

Figure 7.1(b) The position of sample B1 to B6

7.2 Deposition rate

The deposition rate is simply obtained by the ratio from the thickness and the total deposition time.

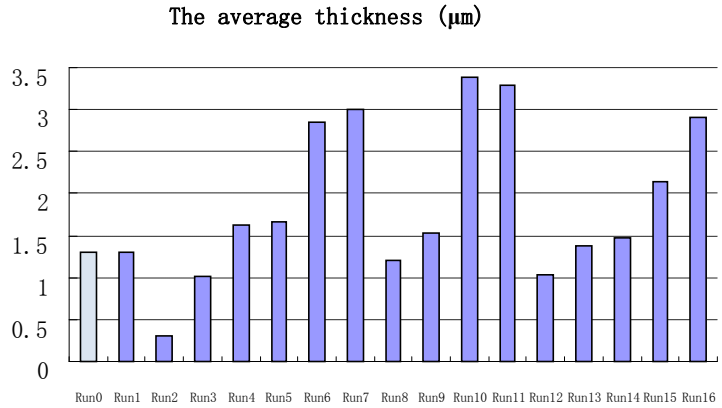

Figure 7.2 The average thickness of Nb thin films

In the superconductivity laboratory we use the HIPIMS technique for the first time in the Nb thin films deposition. We try to obtain films with thickness of 2 μm for each run, but it was very difficult to provide the deposition rate and set the right deposition.

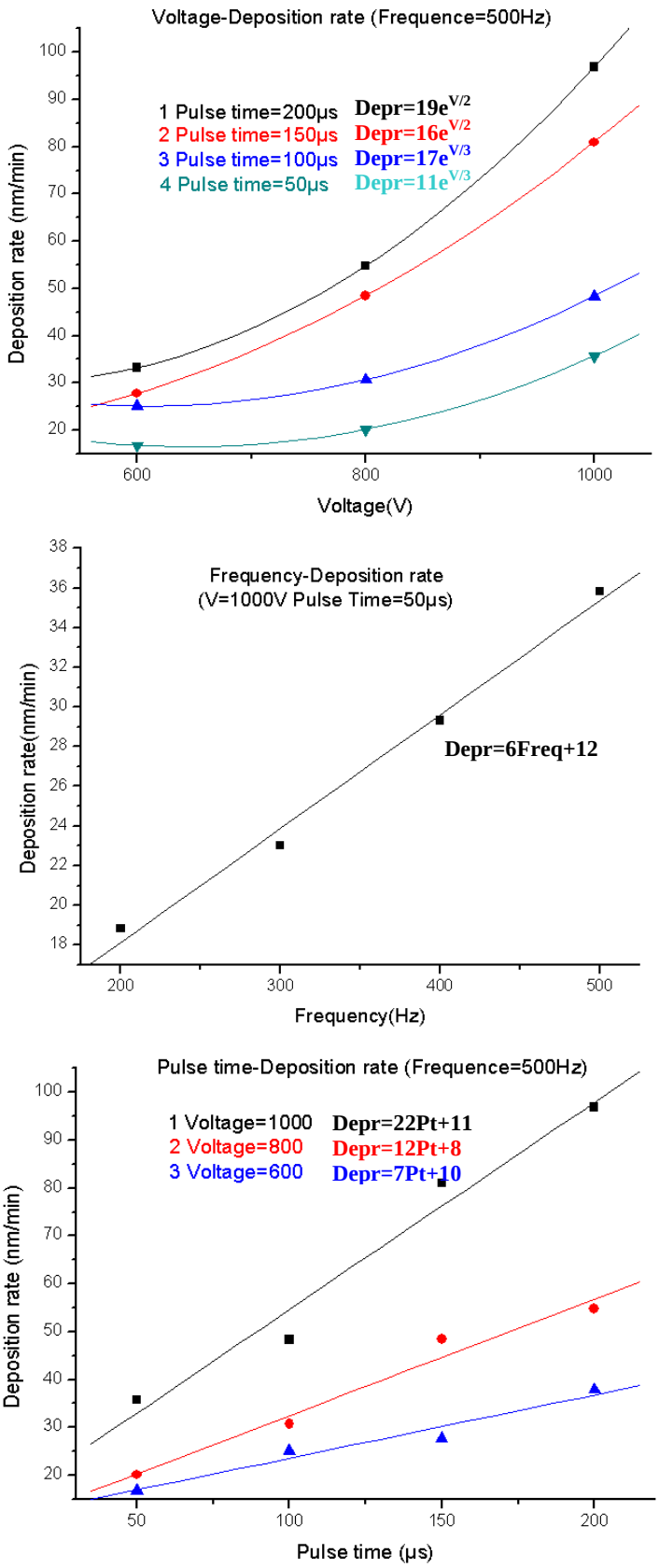

Figure 7.3 The relationship of pulse time, frequency, voltage and deposition rate (Depr=deposition rate; V=voltage; Freq=frequency; Pt=pulse time)

The result is the deposition rate increases with all of these three parameters: voltage, frequency and pulse time increase.

In particular the relationship with frequency and pulse time are linear, meanwhile increment in deposition rate with voltage goes exponentially.

7.3 Microstructure Analysis

Use XRD to measure, the size of crystalline grains and reticular parameters of crystal of Nb thin film was measured with XRD.

For each run the reticular parameter a110, a200 and a211 was measured and calculated from the XRD spectra. From these 3 values we obtain an average reticular parameter (**a**) and grain size D.

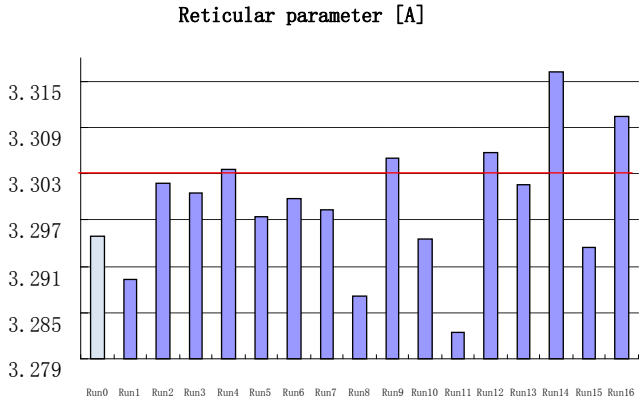

Figure 7.4 The results of reticular parameters

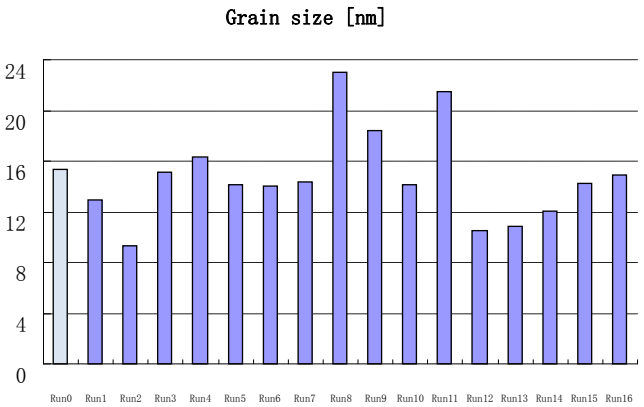

Figure 7.5 The results of grain sizes

Most reticular parameters (a) are less than bulk Nb, so the thin film has a compressive tension.

The relationship of pulse time, frequency, voltage with reticular parameter is shown next below. From the results, when pulse time is 100 μ s all the 3 runs fits very well bulk Nb reticular parameter. For the other parameters is hard suppose a correlations.

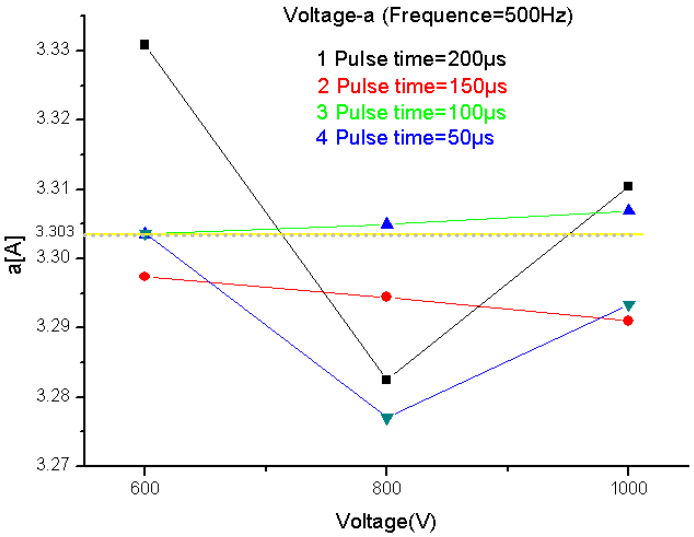

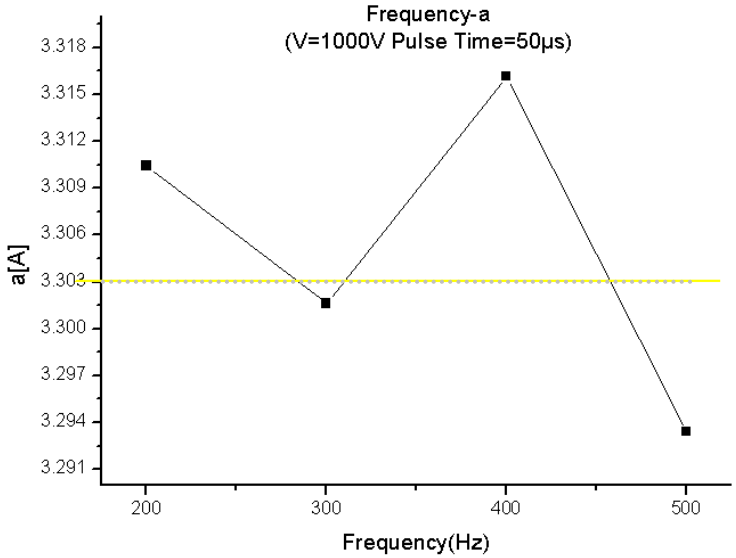

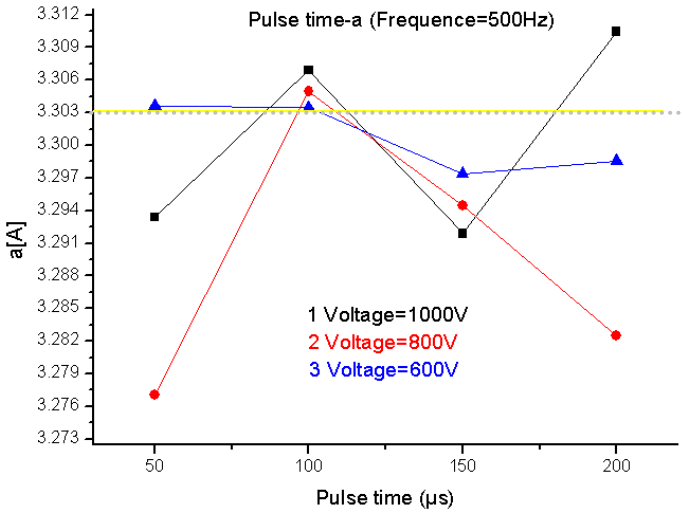

Figure 7.6 The relationship of pulse time, frequency and voltage with reticular parameter (a)

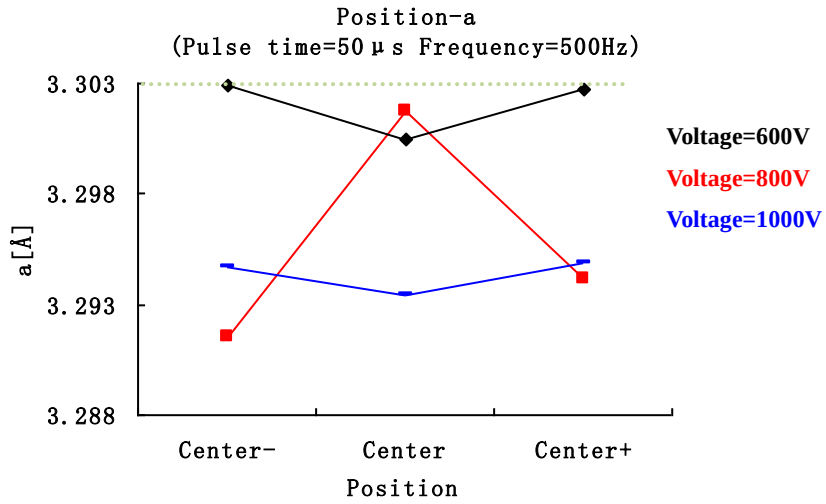

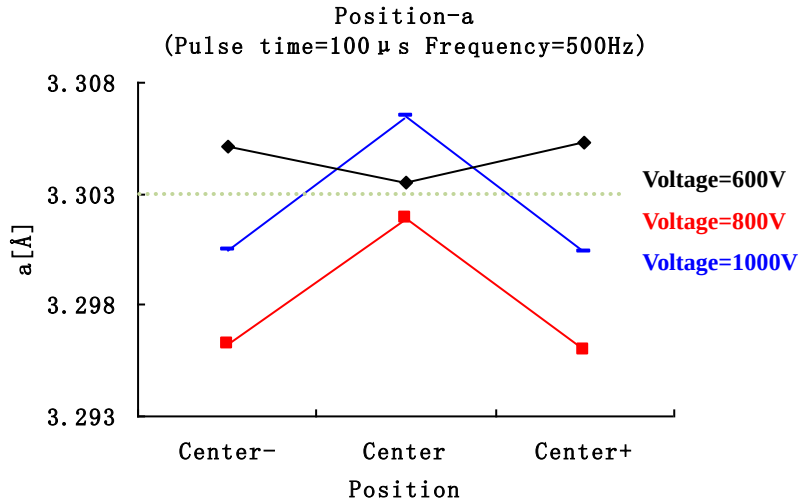

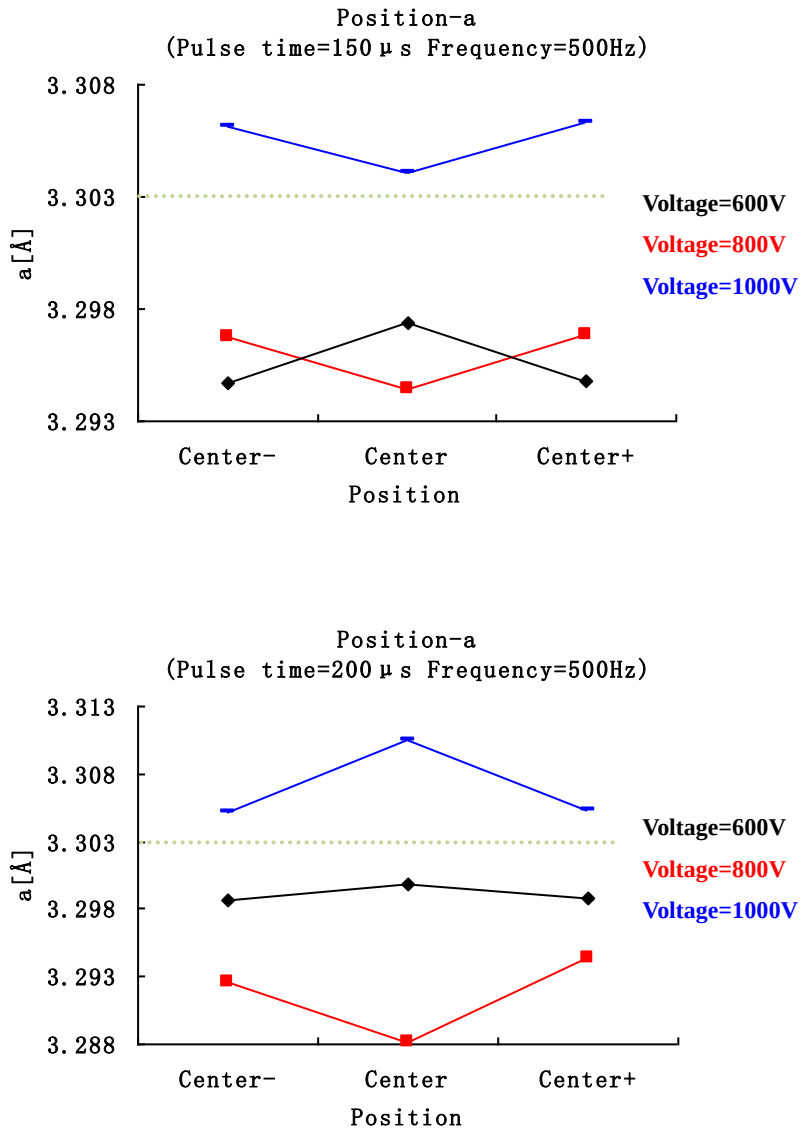

Figure 7.7 The relation of position and reticular parameters (a)

From the result, we can assert that for voltage lower than 800V (except one run at 50 μs pulse time where, however, the values are close to bulk values) the reticular parameters (a) is lower than bulk Nb reticular parameter. When voltage is 1000V, the reticular parameters (a) is higher than bulk Nb reticular parameter (except, also in this case, when pulse time is 50 μs).

In the next page we correlate grain dimension with voltage, frequency and pulse time.

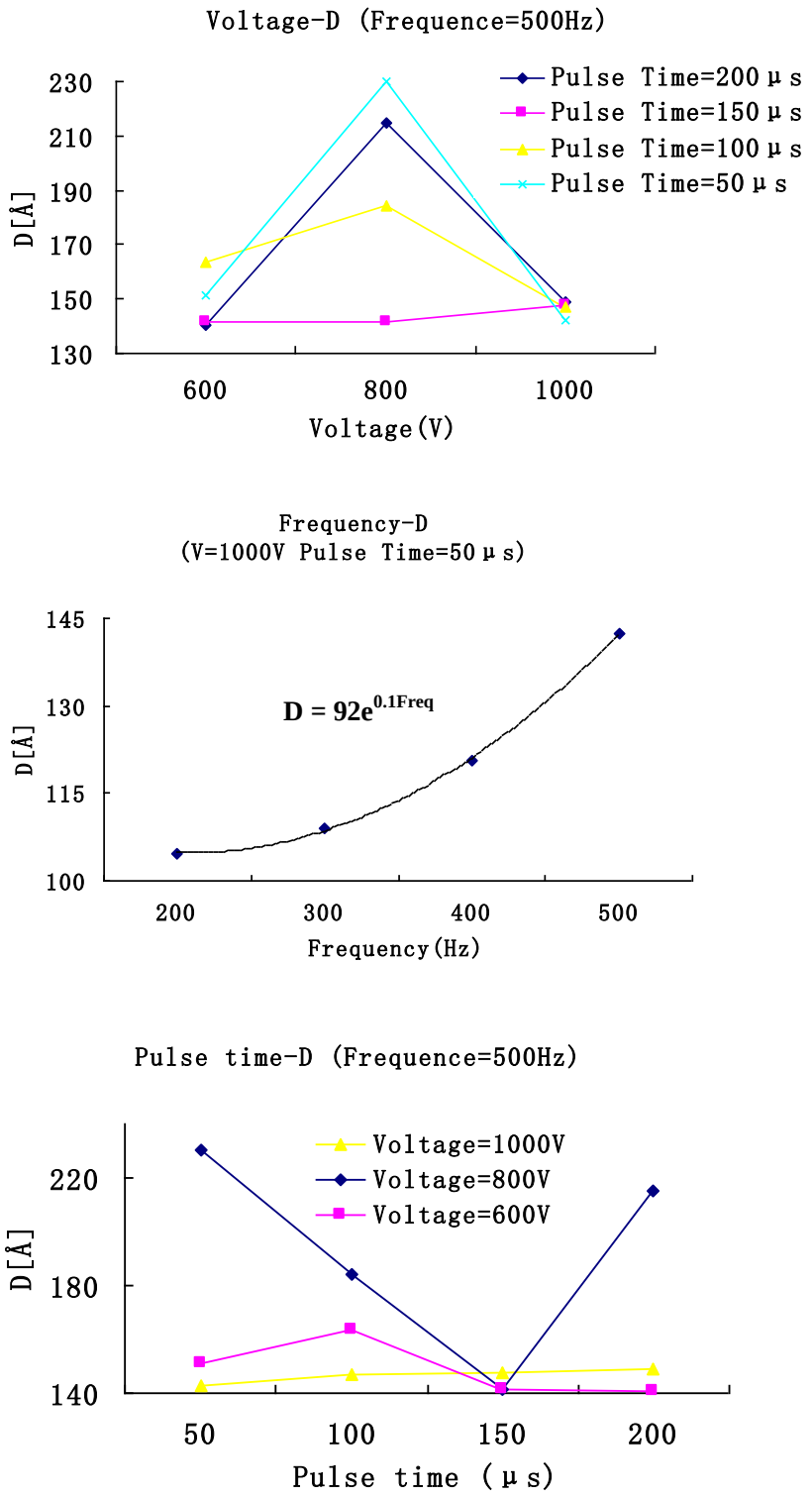

Figure 7.8 The relationship of pulse time, frequency and voltage with grain size (D) (Freq=frequency)

From the results, we can see a maximum in grain dimension when voltage is 800V and a minimum for 150 μs of pulse time. Very interesting is the behavior with frequency: grain dimension exponentially increase with frequency.

7.4 Superconducting Properties

The superconducting properties of the samples are not yet good. Both the T_c and RRR are lower than needed. Also, run0, that is our standard (coated in DC mode) present RRR lower than 10, and T_c less than T_c of bulk Nb. Normally, cavities have RRR more than 20.

Tc of bulk niobium is 9.26K. The experiment results are the following:

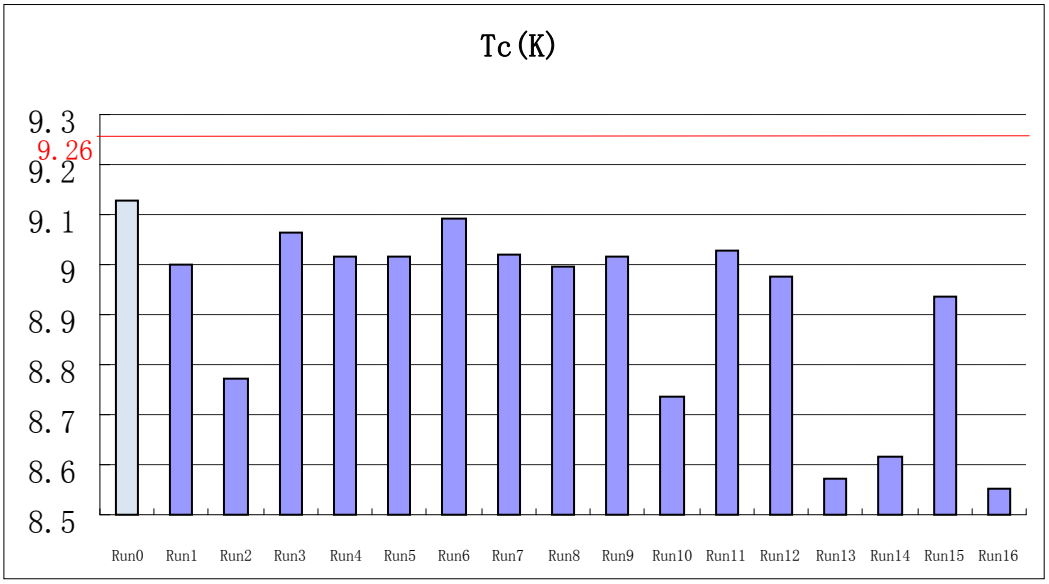

Figure 7.9 The result of Tc of Nb thin film

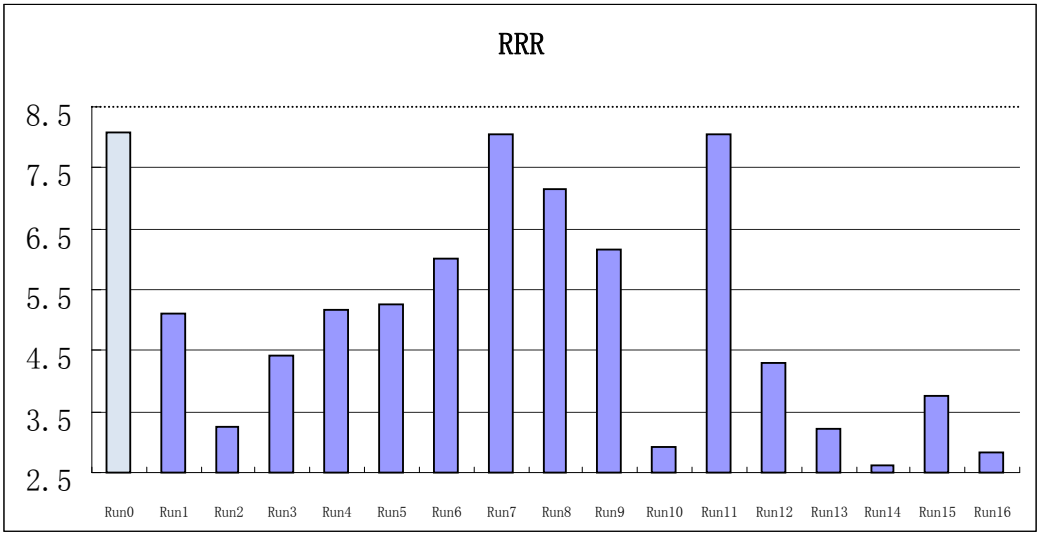

Figure 7.10 The result of RRR of Nb thin film

The possible causes for a Tc lower than bulk Nb is:

1st, degassing of the cavity due to the high temperatures;

2nd, diffusion in the film of niobium atoms of silicon and oxygen from the quartz substrate;

3rd, electron bombardment of the film growth; target of niobium polluted.

We correlate the RRR and the thickness.

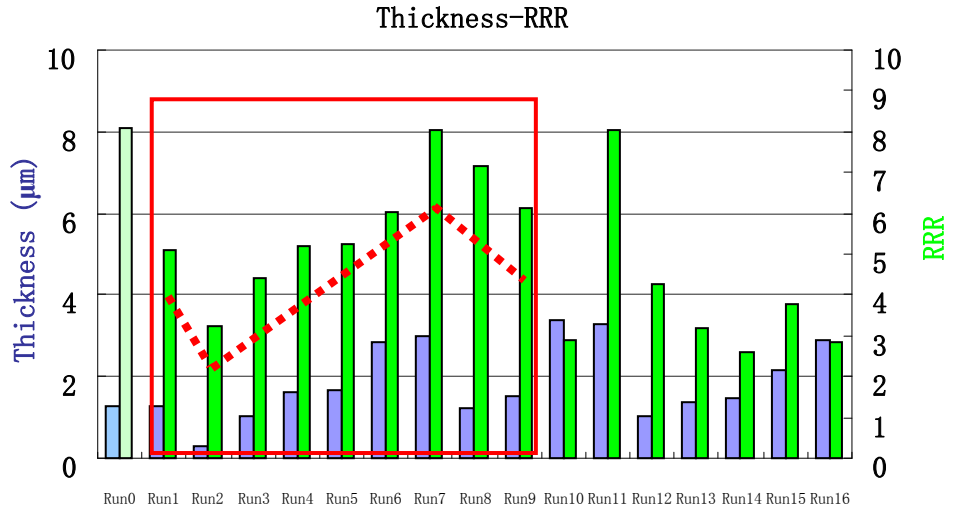

Figure 7.11 The relationship between thickness and RRR

From run1 to run8, the thickness of the film influences the RRR very much. There is a correlation between these two parameters when the film thickness is lower than 1,5 μm.

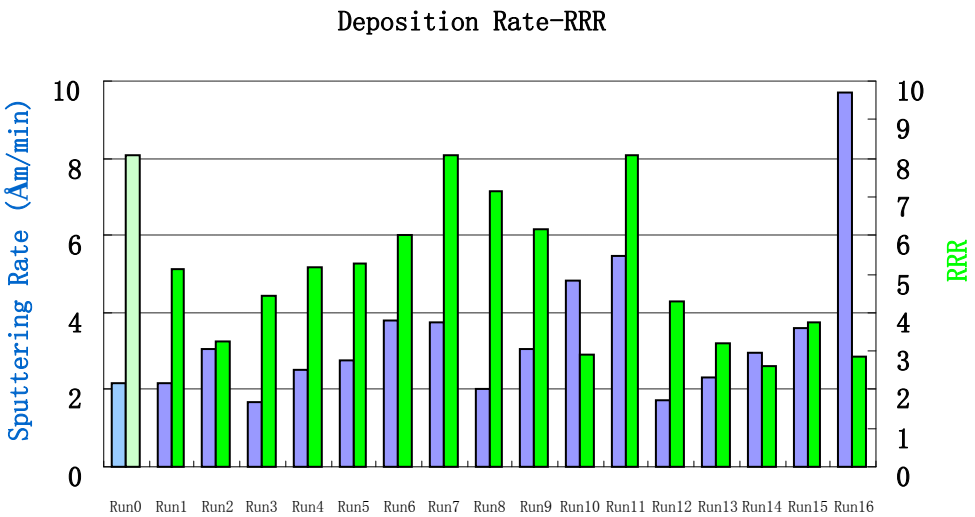

Figure 7.12 The relationship between deposition rate and RRR

From the figure 7.11, there is no correlation between deposition rate and RRR. Only for run 3 to 6 there is a same behavior, but it come from the thickness influence (see figure 7.11).

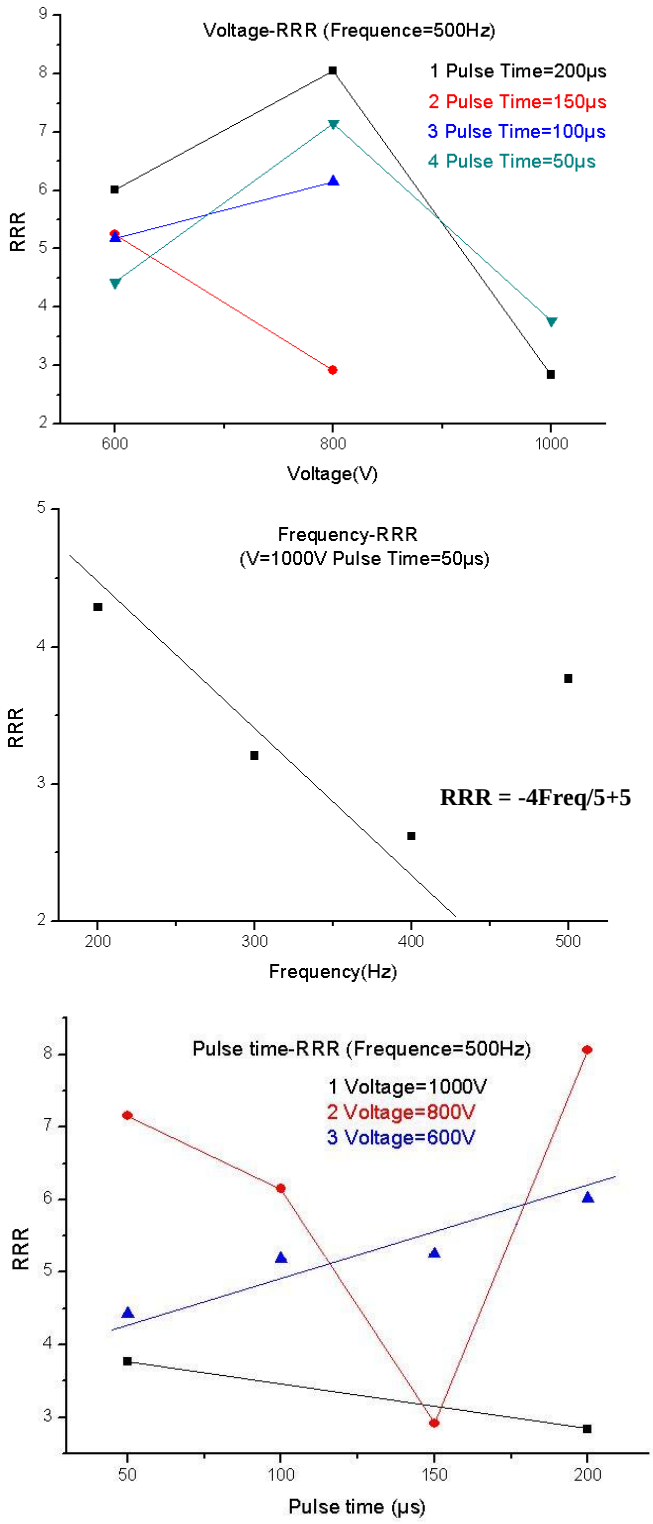

Figure 7.13 The relationship of pulse time, frequency, voltage and RRR

In the previous page we correlate the RRR with voltage, frequency and pulse time. From this graphs we arrive at the following considerations.

Voltage-RRR relationship: except for run 10[1] data, there is a maximum in RRR for 800V voltage, then RRR decreases at very low values for 1000 V. We obtain the same behavior with grain size.

Frequency-RRR relationship: RRR decreases linear with frequency. This behavior is inverse respect grain dimension (see figure 7.8). We remove 500 Hz point from the analysis, because in run 15 RRR is influenced from the thickness. 200, 300, 400 Hz had thickness lower than 1.5 μm; 500 Hz data have thickness higher than 2 μm. This means that the thickness uniformity is very important if you want to understand the behavior of the RRR.

Pulse time-RRR relationship: we haven't found relationship between pulse time and RRR.

[1] *(Voltage=800V, Pulse time=150μs, Frequency=500Hz). In this run the BN insulator was changed. The high degassing of this new important part is probably the reason of the very low RRR.*

8 Conclusions

During this work, HIPIMS have been developed to improve the quality of the niobium film on copper. Finally, will be to transfer it to the deposition of cavities. Preliminary tests were performed to understand the behavior of HIPIMS and the parameters of the relationships between input and output.

The problem is to be suitable for works at high temperatures. Now, for each run, we must stop when the temperature up to 200 degree (baking temperature is 220 degree). And for such a high power, it is very easy to reach that temperature.

After each run, we characterize the film from the point of view of microstructure properties and superconducting properties.

The values of RRR and Tc of deposited films were found to be quite low. There are some possible causes, such as degassing of the cavity due to the high temperatures, diffusion in the film of niobium atoms of silicon and oxygen from the quartz substrate, electron bombardment of the growing film, target of niobium polluted, etc.

We tried to correlate voltage, frequency and pulse time with microstructure and superconductive properties and we found some characteristic behaviors:

1. the deposition rate increases with all of these three parameters: voltage, frequency and pulse time increase. In particular the relationship with frequency and pulse time are linear, meanwhile increment in deposition rate with voltage goes exponentially.
2. Most reticular parameters are lower than bulk Nb value, so the thin film has a compressive tension.
3. From the results, we can see a maximum in grain dimension when voltage is 800V and a minimum for 150 μs of pulse time. Very interesting is the behavior with frequency: grain dimension exponentially increases with frequency.
4. The thickness of the film influences the RRR very much. There is a correlation between these two parameters when the film thickness is lower than 1,5 μm.

5. *Voltage-RRR relationship:* there is a maximum in RRR for 800V voltage, then RRR decreases at very low values for 1000 V. We obtain the same behavior with grain size.
6. *Frequency-RRR relationship:* RRR decreases linearly with frequency. This behavior is opposite to the one shown by grain dimension (see figure 7.8). We remove 500 Hz point from the analysis, because in run 15 RRR is influenced from the thickness. 200, 300, 400 Hz had thickness lower than 1.5 μm; 500 Hz data have thickness higher than 2 μm. This means that the thickness uniformity is very important if you want to understand the behavior of the RRR.
7. *Pulse time-RRR relationship:* we haven't found relationship between pulse time and RRR.

Suggestions for further research:

1st A more efficiently cooling system for the cavity; a cooling water chamber will be done to put the cavity inside to have a better cooling condition.

2nd, A bias will be added to improve superconducting properties. The bias permits to lead the Nb ions produced during the HIPIMS discharge.

3rd, Use SIMS analysis for silicon and oxygen diffuse in the film by quartz or use sapphire substrates in place of quartz to prevent the spread of silicon and oxygen in the film growth;

4th, Analyze the target in order to verify the value of RRR and Tc.

Will HIPIMS be the right technique for Nb/Cu coated 1.5 GHz SC Cavities?

At the end of this preliminary work with HIPIMS I will try to answer to the difficult question on the title of thesis.

We didn't arrive to obtain high values of RRR for our samples, maximum values was around 9. But also in DC mode we obtained the same results in the same system, so this means it's not a problem of technique, but there is something wrong in our deposition system. We talked about it before: the uncooled cathode and high temperature reached by the cavity during the process are the principal candidates of the film pollution. On the other hands we found that HIMPIMS parameters (in particular voltage and frequency) influence the microstructure and the RRR of the coated films. This means that if we found the right deposition parameters we would obtain a high quality superconductive film.

At the moment the goal it is to identify and solve the problem of pollution of the film, in order to obtain high RRR values. Only after having obtained high purity films, HIPIMS can be studied deeply and used for deposition of the entire surface of the cavity. After that the second stage of optimization of the deposition will be possible to deposit a copper cavity and measure the features.

Acknowledgements

I would like to acknowledge my supervisor: **Prof. V. PALMIERI**, for giving me the great opportunity to study and work on sputtering and superconducting cavities, making me progress, and most of all for believing in me to explore HIPIMS of Nb for superconducting cavities.

I would like to acknowledge my Assistance supervisor: **Dr. CRISTIAN PIRA,** for directing me to work and answering my questions, giving me the freedom to do the experiments and helping me a lot on the thesis.

I would also like to thank my colleagues and friends in the Surface treatments laboratory together: Silvia MARTIN, Giorgio KEPPEL, Winder GONZALEZ, Oscar AZZOLINI, Antonio ROSSI, Vanessa RAMPAZZO, LI Jinhai, Dmytro CHIRKOV, Hanieh JAHAN FAR, Iman MORADI, Giovanni TERENZIANI, and Gabriela ACOSTA.

I am fortunate to have been working among so many talented people.

Last but not the least, I am very grateful towards my family and friends, the ones who are still around and the ones who departed, for all the support and love you have given me throughout all these years.

References

[1] Livingston, M. Stanley & Blewett, John, Particle Accelerators, New York: McGraw-Hill, (1962)
[2] Widerøe, R. (subscription required) Archiv Elektronik und Uebertragungstechnik 21: 387, (1928)
[3] H. Padamsee, Superconducting Sci.Technol. 14 (2001) R28–R51.
[4] Sanjay Malhotra, Method For Measuring Residual Resistivity Ratio (RRR) on Standard C Bench using Keithley voltmeters
[5] B. Bonin, Materials for superconducting cavities, in: Superconductivity in Particle Accelerators, S. Turner, CERN, May 1996, p. 191, CERN 96-03.
[6] K. Saito, P. Kneisel, Temperature Dependence of the Surface Resistance of Niobium at 1300 MHz - Comparison to BCS Theory, in: Proceedings of the 9th Workshop on RF Superconductivity, Santa Fe, New Mexico, USA, (1999)
[7] J. Halbritter, Calculation of the BCS surface resistance, Z. f.Phys. 238 (1970) 466.
[8] 2004 CERN Accelerator School: Superconductivity and cryogenics for accelerators and detectors
[9] 1996 CERN Accelerator School: Superconductivity in particle accelerators
[10]1989 CERN Accelerator School: Course on superconductivity in particle accelerators
[11]B. Aune et al., "Superconducting TESLA cavities", Phys. Rev. ST Accel. Beams 3, 092001 (2000). A thorough presentation of the many aspects of an SRF cavity
[12]2009 Conference on RF Superconductivity
[13]SRF Tutorials at the 2009 Conference on RF Superconductivity
[14] Wutz M., Adam H., Walcher W. and Steckelmacher W. Theory and Practice of Vacuum Technology, Friedrich Vieweg & Sohn Verlag (1989)
[15]R. Behrisch (ed.) Sputtering by Particle bombardment:. Springer, Berlin. ISBN 978-3540105213, (1981)
[16] P. Sigmund, Nucl. Instr. Meth. Phys. Res. B "Mechanisms and theory of physical sputtering by particle impact". Nuclear Instruments and Methods in Physics Research Section B Beam Interactions with Materials and Atoms 27: 1. doi:10.1016/0168-583X(1987)90004-8.
[17]R. Behrisch and W. Eckstein (eds.) Sputtering by Particle bombardment: Experiments and Computer Calculations from Threshold to Mev Energies. Springer, Berlin, (2007)
[18] L. Maissel, R. Glang, Handbook of Thin Film Technology, McGraw-Hill, New York, (1970)
[19] Sturrock, Peter A. Plasma Physics: An Introduction to the Theory of Astrophysical, Geophysical & Laboratory Plasmas.. Cambridge University Press. (1994)
[20] M. Ohring Materials Science of Thin Films, Academic Press, San Diego, CA, USA, (2002)
[21] S.M. Rossnagel in J.L. Vossen and W. Kern (eds.), Thin Film Processes II,

Academic Press, New York, USA (1991)
[22] D.M. Sanders, J. Vac. Sci. Technol. A 7, 2339 (1989)
[23] D. Hoffman, R. McCune, Microstructural control of plasma sputtered refractory coatings, in: S. Rossnagel, J. Cuomo, W. Westwoood (Eds.), Handbook of plasma processing technology, Noyes publications, (1990)
[24] B. Movchan, A. Demchishin, Study of the structure and properties of thin vacuum condenstaes of nickel, titaniom, tungsten, aluminium oxide, and zirconium oxide, Fiz.Metal.Metalloved 28 (1969) 653.
[25] L. Maissel, P. Schaible, Thin Films Deposited by Bias Sputtering, J.Appl.Phys. 36 (1965) 237.
[26] J. Thornton, Influence of apparatus geometry and deposition conditions on the structure and topography of thick sputtered coatings, Journ. of Vacuum Sci. and Tech. 11 (1974) 666.
[27] A. C. Raghuram, R. F. Bunshah, Journ. of Vacuum Sci. and Tech. 9 (1974) 1389.
[28] G. Orlandi, C. Benvenuti, S. Calatroni, F. Scalambrin, Expected dependence of Nbcoated RF cavity performance on the characteristics of niobium, in: Proceedings of the 6th Workshop on RF Superconductivity, CEBAF, USA, (1993)
[29] G. M. Schucan, C. Benvenuti, S. Calatroni, Niobium films produced by magnetron sputtering using an Ar-He mixture as discharge gas, note 94-23.
[30] C. Benvenuti et. al., Rare gas trapping in sputtered Nb films, in: Proceedings of the 7th Workshop on RF Superconductivity, Gif-sur-Yevette, France, (1995)
[31] V. Kouznetsov, K. Macák, J.M. Schneider, U. Helmersson, and I. Petrov, Surf. Coat. Technol. 122, 290, (1999)
[32] K. Macák, V. Kouznetsov, J. Schneider, U. Helmersson, and I. Petrov, J. Vac. Sci. Technol. A 18, 1533, (2000)
[33] V. Kouznetsov, U.S. Patent No. 6,296,742 B1, (2001)
[34] V. Kouznetsov, US Patent 2004/0020760 A1, (2004)
[35] V. Kouznetsov, Swedish Patent 525231, (2005)
[36] V. Kouznetsov, WO 2005/005684 A1, (2005)
[37] A.P. Ehiasarian, R. New, W.-D. Münz, L. Hultman, U. Helmersson, and V. Kouznetsov, Vacuum 65, 147, (2002)
[38] V. Kouznetsov, U.S. Patent No. 6,296,742 B1 (2001)
[39] D.J. Christie, W.D. Sproul, D.C. Carter, and F. Tomasel, Proceedings of the 47th Annual Technical Conference Proceedings of the Society of Vacuum Coaters, 113 (2004)
[40] D.J. Christie, F. Tomasel, W.D. Sproul, and D.C. Carter, J. Vac. Sci. Technol. A 22,1415 (2004)
[41] B.M. DeKoven, P.R. Ward, and R.E. Weiss, D.J. Christie, R.A. Scholl, W.D. Sproul, F. Tomasel, and A. Anders, Proceedings of the 46th Annual Technical Conference Proceedings of the Society of Vacuum Coaters, 158, (2003)
[42] W.D. Sproul, D.J. Christie, and D.C. Carter, Proceedings of the 47th Annual Technical Conference of the Society of Vacuum Coaters, 96, (2004)
[43] J. Alami, Dissertation No 948, Linköping Studies in Science and Technology, (2005)

[44] J. Alami, P.O.Å. Persson, D. Music, J.T. Gudmundsson, J. Bohlmark, and U. Helmersson, J. Vac. Sci. Technol. A 23, 278, (2005)
[45] A.P. Ehiasarian et al., Vacuum 65 (2002) 147154
[46] J. Alami et al., J. Vac. Sci. Technol. A 23 (2005) 278
[47] J. Alami et al., Thin Solid Films 515 (2006) 1731
[48] C. Benvenuti et al., Physica C 316 (1999) 153
[49] S.P. Bugaev, N.N. Koval, N.S. Sochugov, and A.N. Zakharov, Proceedings of the XVIIth International Symposium on Discharges and Electrical Insulation in Vacuum, 1074, (1996)
[50] J.A. Davis, W.D. Sproul, D.J. Christie, and M. Geisler, Proceedings of the 47th Annual Technical Conference Proceedings of the Society of Vacuum Coaters, 215, (2004)